Section 1

Atmospheric data assimilation schemes, analysis and initialization, data impact studies, observing system experiments

Upgrade to 4D-Var of the operational ensemble variational assimilation at Météo-France

L. Berre, G. Desroziers, L. Raynaud,
METEO-FRANCE (CNRM/GAME), Toulouse, France

Data assimilation is based on a statistical characterization of forecast errors. One needs to specify expected amplitudes of these errors (described by variances), which depend on the weather situation.

In this context, a real time ensemble variational assimilation system (AEARP) has been running operationally at Météo-France since July 2008 (Berre et al 2007, 2009), by using six perturbed 3D-Var FGAT assimilations. The spread of such an ensemble allows the space and time dynamics of background errors to be estimated, and resulting background error variances “of the day” are used as an input to the (unperturbed) 4D-Var system. Moreover, a 4D-Var version of this ensemble assimilation is experimented, in order to better simulate errors of the 4D-Var system.

This is illustrated by figures a, b and c, which correspond to a severe storm case over France (figure c), on 24 January 2009. The geographical distribution of variances is more realistic in the 4D-Var version (figure a) than in the 3D-Var version (figure b), with a maximum which is more pronounced and better located over France, in accordance with the strong uncertainty associated to this kind of intense weather system.

The superiority of the ensemble 4D-Var assimilation has been confirmed by comparisons with departures between observations and forecasts, and by impact studies of variances, provided by the ensemble, on the forecast quality. The associated increase of computation cost is moderate, and compatible with the ongoing computation power increase. This upgrade will become operational in the first half of 2010.

In terms of perspectives, it is planned to extend the use of departures between observations and forecasts, to estimate contributions of model errors (to be distinguished from errors induced by initial conditions). This will enable to estimate this error component objectively, as it is poorly known currently.

CAPTION OF THE FIGURE ON NEXT PAGE

Maps of standard deviations of background errors of zonal wind (unit : ms^{-1}) around 500 hPa, on 24 January 2009 at 03 UTC, estimated with two different versions of ensemble assimilation. (a) : standard deviations provided by an ensemble 4D-Var assimilation ; (b) : standard deviations provided by an ensemble 3D-Var assimilation. The mean sea level pressure field at 00 UTC is shown in panel (c).

REFERENCES

Berre, L., O. Pannekoucke, G. Desroziers, S.E. Stefanescu, B. Chapnik and L. Raynaud, 2007: A variational assimilation ensemble and the spatial filtering of its error covariances: increase of sample size by local spatial averaging. Proceedings of the ECMWF workshop on flow-dependent aspects of data assimilation, 11-13 June 2007, 151-168. (available on line at: http://www.ecmwf.int/publications/library/do/references/list/14092007)

Berre, L., G. Desroziers, L. Raynaud, R. Montroty and F. Gibier, 2009: Consistent operational ensemble variational assimilation. Extended abstracts of the Fifth WMO International Symposium on Data Assimilation, Paper N.196.

(a)

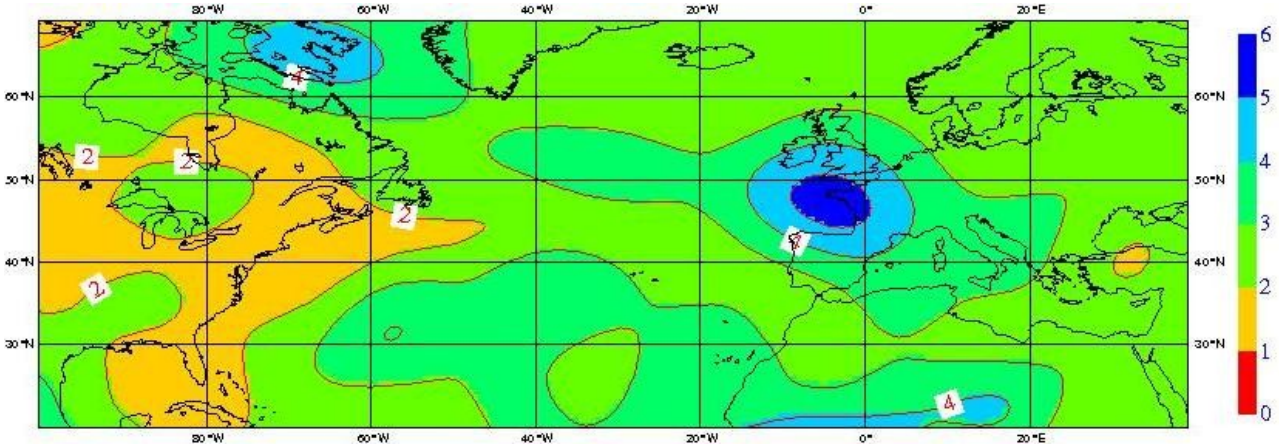

(b)

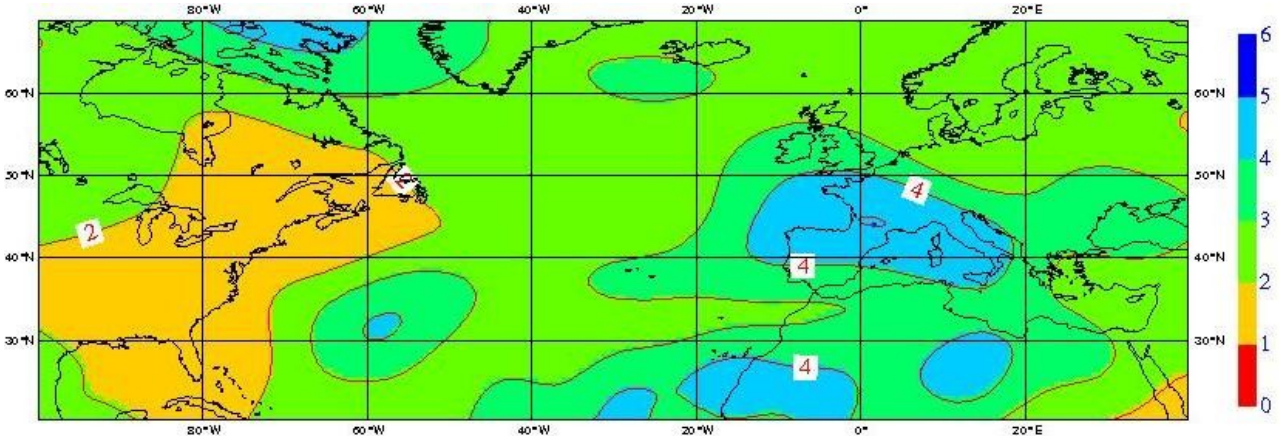

(c)

ANASYG du SAM 24/01/2009 00 UTC

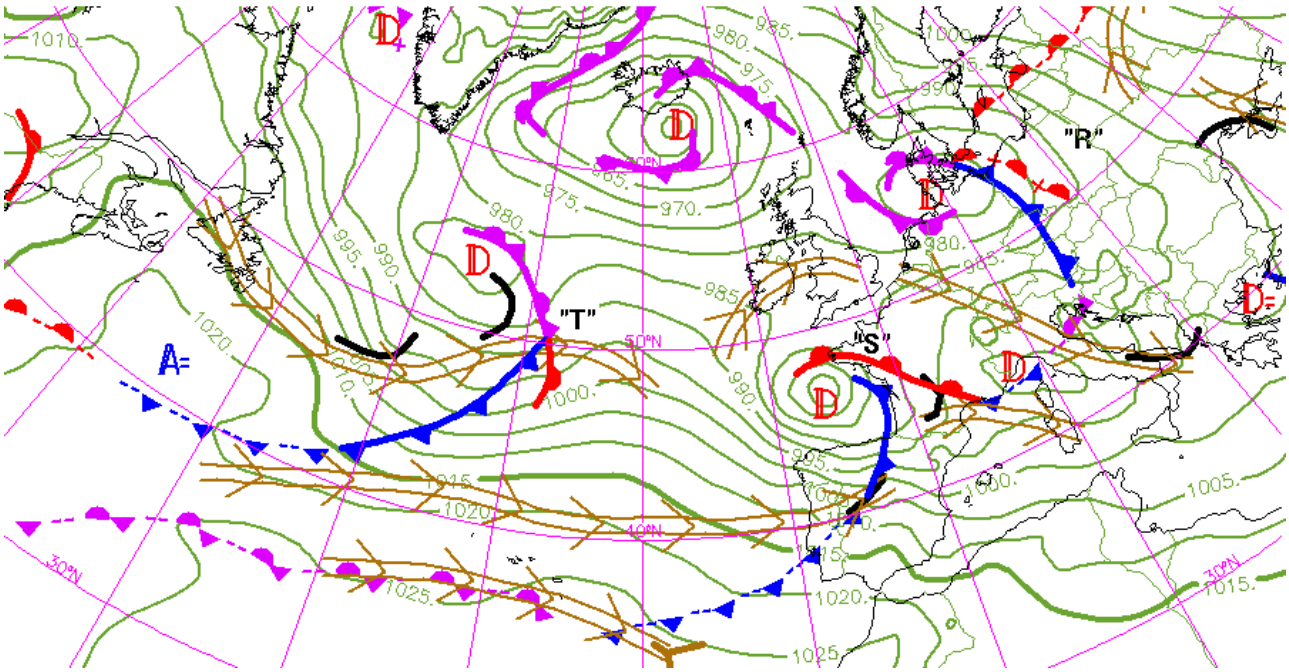

Assimilation of Synthetic Aperture Radar (SAR) wind information in Environment Canada's high-resolution 3D-Var analysis system

Rick Danielson (@ec.gc.ca), Luc Fillion, and Harold Ritchie
Meteorological Research Division (Dorval), Environment Canada

1. Introduction

The potential benefit of assimilating SAR data into an atmospheric model is generally difficult to take advantage of in conventional assimilation cycles. One challenge lies not so much with the O[1-km] resolution of the numerical model itself, but with the resolution employed when combining observations with a previous forecast to produce the next set of initial conditions (i.e., the analysis increments that define the state vector in our assimilation approach). This resolution is determined largely by the model error covariance matrix. Here, we employ a limited-area version of the Global Environmental Multiscale (GEM) model (Cote et al. 1998).

2. A limited-area 3D-var system

Data assimilation at Environment Canada has traditionally been global with analysis increments at about 180-km resolution. The newest operational system (Fillion et al. 2010) will employ a 55-km limited-area grid. Experimental subdomains with analysis grids at close to 2.5-km resolution are also now possible within the unified 3D-Var code. These employ a bi-Fourier representation of the GEM errors that is analogous to the spectral representation used for global assimilation.

3. High-resolution model errors

The GEM 3D-var error correlations are horizontally homogeneous and isotropic for all wavenumbers of a limited-area domain. They have non-separable vertical and horizontal components for the Helmholtz wind decomposition (ψ, χ), temperature (**T**), and humidity (**logQ**). Error structures are derived using the so-called NMC method (Parrish and Derber 1992), which assumes that a difference in two forecasts (both valid at the same time, but starting from 12-h and 36-h beforehand, for example) is representative of a model error. Ensembles of high-resolution GEM forecasts (~120) have been employed in experiments to date.

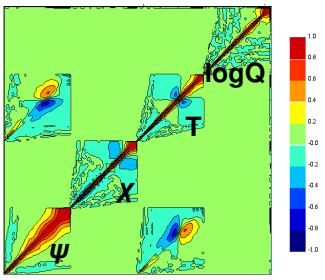

Fig. 1a: Typical vertical correlation matrix at the 2000-km (synoptic) scale (lower left corner of each block is at the GEM model top). Geostrophic and hydrostatic balance is reflected (in spite of the fact that no error balance is assumed).

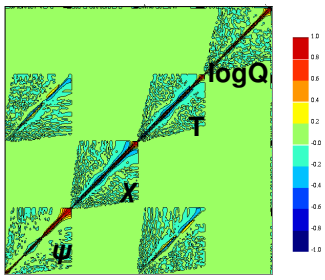

Fig. 1b: At a scale of 200-km, there is much less spatial autocorrelation and the larger scale balance is not as evident (this is expected). Not yet included here is the cross-correlation of Helmholtz variables (ψ, χ) to capture low-level Ekman pumping.

4. Analysis example

A Radarsat-2 ScanSAR HH-polarized scene (Fig. 2a) captured the signature of high winds south of Newfoundland on 10 February 2009, in the wake of a cyclone. Wind streaks are apparent in the SAR image, but only backscatter was considered in an analysis experiment that set SAR errors at 2% of backscatter in dB and neglected spatial error covariance (which was likely important). The impact of surface SAR backscatter on the analysis increments of temperature and wind are shown in Fig. 2b at about 2km above the surface. Maximum values are ¼ degrees (colours) and 5 knots (vectors). The SAR impact here is to increase the wind speed and produce quasi-balanced large-scale temperature changes.

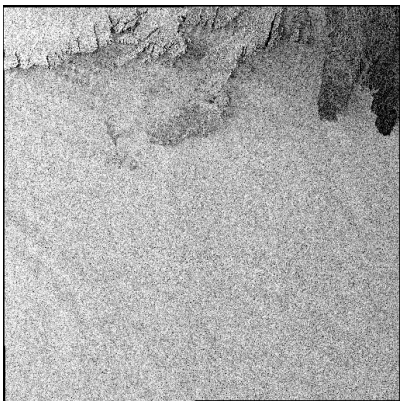

Fig. 2a: Radarsat-2 SAR backscatter

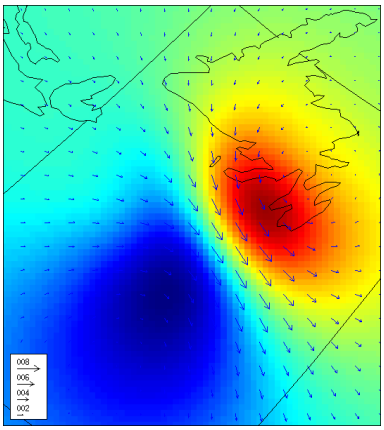

Fig. 2b: Analysis increments

5. Conclusions

An appropriate framework exists for testing the impact of SAR assimilation in Environment Canada's limited-area variational data assimilation system (Fillion et al. 2010). This system is being employed to define the GEM error covariance matrix (B). Incorporation of previous offline results (Danielson et al. 2008) in an experimental assimilation system is now being conducted. Tests of SAR (versus other satellite) impacts on analyses and forecasts for an east coast region are planned.

6. References

Coté, J., S. Gravel, A. Méthot, A. Patoine, M. Roch, and A. Staniforth, 1998 : The operational CMC-MRB Global Environment Multiscale (GEM) model. Part I: Design considerations and formulation. *Mon. Wea. Rev.,* **126,** 1373-1395.

Danielson R. E., M. Dowd, H. Ritchie, 2008: Objective analysis of marine winds with the benefit of the Radarsat-1 synthetic aperture radar: A nonlinear regression framework, *J. Geophys. Res.,* **113,** C05019, doi:10.1029/2007JC004413.

Fillion, L., M. Tanguay, E. Lapalme, B. Denis, M. Desgagne, V. Lee, N. Ek, Z. Liu, M. Lajoie, J.-F. Caron, and C. Page, 2010: The Canadian regional data assimilation and forecasting system. *Wea. Forecasting,* submitted Jan. 2010.

Parrish, D. F., and J. C. Derber, 1992: The National Meteorological Center's spectral statistical-interpolation analysis system. *Mon. Wea. Rev.,* **120,** 1747-1763.

7. Acknowledgements

This work is being funded by the Canadian Space Agency. SAR data was taken from archives of the Canadian Centre for Remote Sensing.

Assimilation of SSMIS Imager Channels in the JMA's Global 4D-Var Data Assimilation System

Takumu Egawa
Numerical Prediction Division, Japan Meteorological Agency
E-mail: egawa@met.kishou.go.jp

The Japan Meteorological Agency (JMA) started to assimilate clear radiance data from the DMSP-F13/14/15/SSM/I, TRMM/TMI and Aqua/AMSR-E spaceborne microwave imagers in the operational global 4D-Var data assimilation system with a variational bias correction scheme in May 2006. The assimilated channels were four vertically polarized channels of SSM/I and the corresponding channels of TMI and AMSR-E (Sato 2007).

The SSMIS on board DMSP-F16/17 is the successor to the SSM/I series. Figure 1 shows statistics for the O-B (the observed brightness temperature minus the calculated brightness temperature from the background). The quality of the SSMIS imager channels is comparable to that of SSM/I after air-mass bias correction.

Experiments for an impact study were performed using JMA's low-resolution global data assimilation system (TL319L60) and forecast model. The assimilated channels were 19V, 22V, 37V and 92V. The horizontally polarized channels were not used, as the vertical polarized channels contain almost the same information under the current standard for assimilation of surface emissivity. The wind speed Jacobian is not considered in the radiative transfer model. In our experiments, SSMIS imager channels had a positive impact on the analysis fields for 850-hPa temperature and water vapor, while the impact on forecasts for 500-hPa geopotential height was neutral.

In line with these results, JMA started using SSMIS imager radiance data on board DMSP-F16 and F17 in operational global 4D-Var analysis from March 2009.

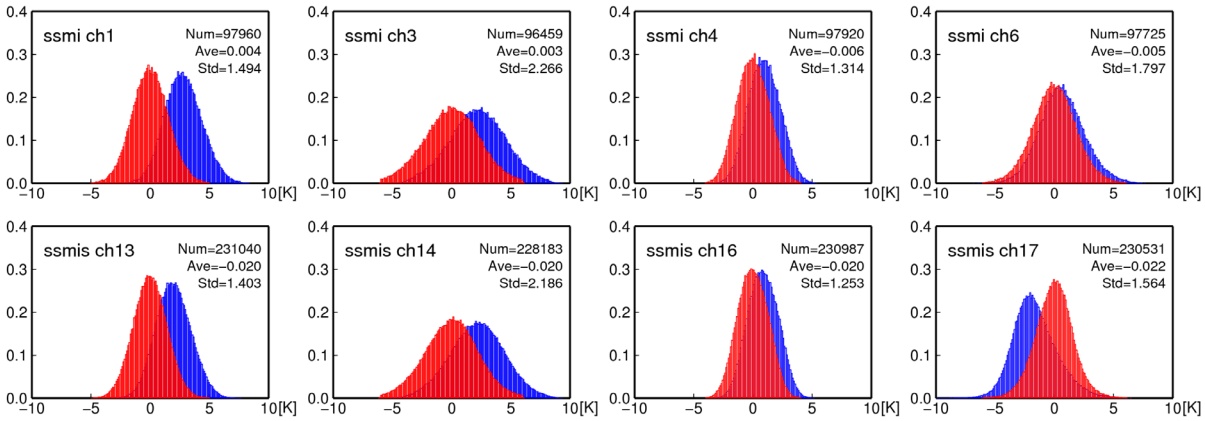

Figure 1. O-B statistics for DMSP-F13/SSM/I (ch. 1, 3, 4, 6) and DMSP-F16/17/SSMIS (ch. 13, 14, 16, 17). The red histogram areas are for after air-mass bias correction, and the blue ones are for before.

References

Sato, Y., 2007: Introduction of spaceborne microwave imager radiance data into the JMA global data assimilation system, *CAS/JSC WGNE Res. Activ. Atmos. Oceanic Modell.*, **37**, 01.17 – 18.

Impact of hyperspectral infrared sounders in Numerical Weather Prediction models of Meteo-France

Nadia Fourrié,Vincent Guidard and Florence Rabier
CNRM/GAME, Météo-France and CNRS
42 av Coriolis
31057 Toulouse
France
Nadia.Fourrie@meteo.fr

As of early 2010, the operational global spectral forecasting model of Météo-France called "ARPEGE" runs four times a day with 60 levels in the vertical and a variable T538 horizontal resolution enabling a 15 km grid resolution over France, decreasing to 90 km at the antipodes. The data assimilation system is a Four-Dimensional Variational scheme (4DVAR), performed on 6h time windows. Météo-France also operates a 3DVAR assimilation (6h cycling) to initialize a limited-area model called "ALADIN-FRANCE" at 9 km horizontal resolution and a new fine-mesh model called "AROME" at 2.5km horizontal resolution over France. IASI and AIRS, respectively onboard the European MetOp and US Aqua polar orbiting satellites, are hyperspectral infrared sounders which provide thousands of channels in each profile. They are used operationally in the global model ARPEGE and the limited-area model ALADIN since 2006 for AIRS and 2008 for IASI with a horizontal sampling of 250 km. However, only a subset of channels is used in the data assimilation. 54 channels are assimilated for AIRS over open sea and the number of IASI assimilated channels depends on the surface type: 64 over open sea, 50 over land and 32 channels over sea ice. These channels provide information on temperature roughly from 50 hPa down to 650 hPa.

In April 2010, the assimilated satellite data number have been increased by enhancing the horizontal sampling of the observations in the 3 operational models. In the global model ARPEGE, to assimilate 4 times more data, from 1 every 250 km to 1 every 125km, has shown a positive impact on forecasts for all variables and at all forecast ranges. The number of assimilated channels has also been increased for the IASI sounder. Four surface channels have been added over the sea for clear sky observations and 9 water vapour channels sounding in the upper-troposphere are assimilated over land and over the sea, leading to slightly positive impact on humidity for short forecast ranges (up to 24 hours).

As infrared spectra are strongly affected by the presence of clouds, their detection and characterization are of prime importance. At first, only clear channels were assimilated in the numerical weather prediction models. However, the sensitive areas where the cyclogenesis occur are mostly cloudy. In order to take into account the cloud effects in the simulation of the observation, a CO2slicing algorithm is used to retrieve a cloud-top pressure and a cloud fraction, which are then fed into the system to assimilate cloud-affected channels. This has been evaluated for AIRS spectra and led to an increase of the amount of used data and also to a positive impact on forecasts. Similar developments are in progress for IASI. As an example, figure 1 exhibits the cloud top pressure retrieved from IASI for the 24th of January 2009 around 00 UTC, when the storm named Klaus was approaching the French coast. The comma cloud shape associated with high level clouds and typical of severe storms is visible in the picture. A front located over the Atlantic Ocean is also seen. Tests of the cloudy IASI radiance assimilation have started in the global NWP model.

IASI and AIRS data have also been assimilated in the convective scale model AROME. Despite a rather poor temporal coverage of the domain, they exhibited a positive impact for upper air and surface fields at all time ranges up to 30h. The prediction of precipitation, which is a key point for AROME, has also been improved as shown by figure 2.

The next steps for the assimilation of hyperspectral souders will consist mainly in increasing their use over the continents and in characterizing land surface properties to enhance the assimilation of infrared sounders over land for all NWP models. Moreover, the horizontal density of spectra used in AROME will be specifically increased.

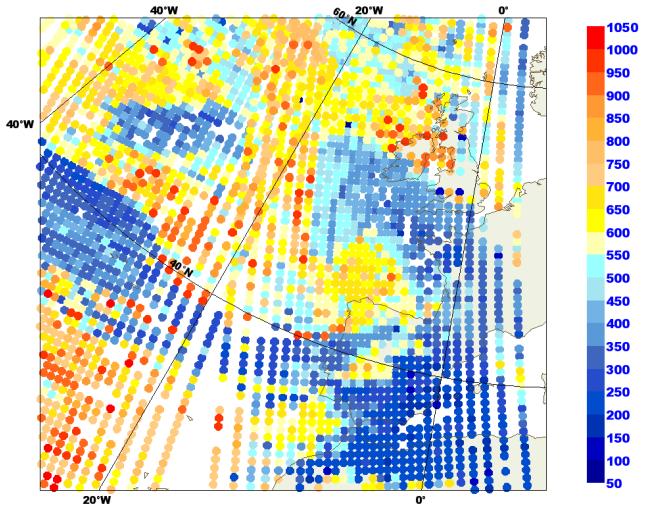

Figure 1: Cloud top pressure (in hPa) retrieved from IASI sounder with the ARPEGE model for the 24 january 2009 at around 00UTC.

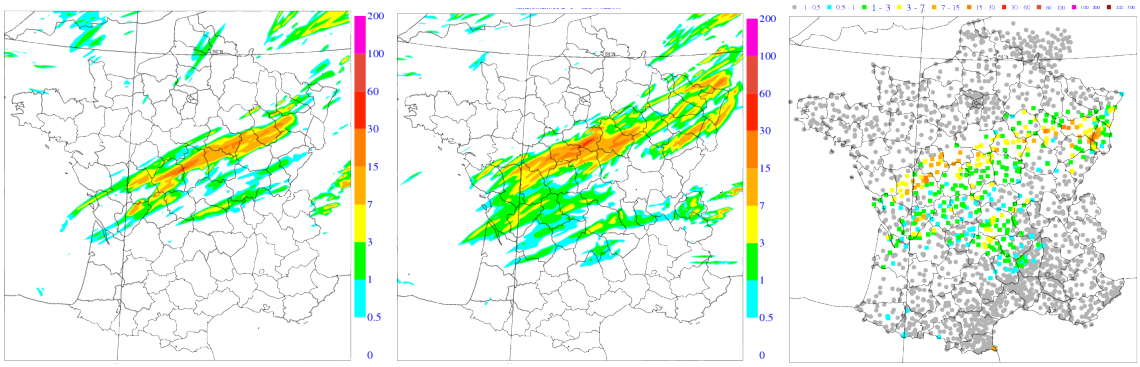

a) b) c)

Figure_2: 12h precipitation accumulation as forecasted by AROME with no assimilation of AIRS nor IASI data (a), and with assimilation of AIRS & IASI data (b), to be compared with rain gauge measurements (c), for the period between 00 and 12 UTC on 21st of May 2009.

Optimization of Error Covariance Matrices and Estimation of Observation Data Impact in the JMA Global 4D-Var System

Toshiyuki Ishibashi
Numerical Prediction Division, Japan Meteorological Agency
1-3-4 Otemachi, Chiyoda-ku, Tokyo 100-8122, Japan
E-mail: ishibasi@met.kishou.go.jp

1. Introduction

Since data assimilation theories based on maximum likelihood estimation such as 4D-Var have error covariance matrices (ECMs) as external parameters, real data assimilation systems (DASs) must have ECMs with a sufficient level of accuracy. The validity of ECMs is one of the main factors in determining the accuracy of analysis fields because they strongly influence the effects of observational data and background fields on analysis fields.

Two methods can be used for ECM optimization. The first is based on Desroziers and Ivanov (2001, QJRMS) and Chapnik (2006, QJRMS), and is referred to here as the DIC method. In DIC, ECMs are tuned to satisfy the theoretical relationships between ECMs and the cost function of 4D-Var, and the method includes evaluation of observation data impacts (ODIs) on analysis fields because it includes calculation of degrees of freedom for signals (DFS) (Rabier, 2002, QJRMS) used in ODI estimation. The second is a method based on Daescu (2008, MWR), and is referred to here as D08. Although this approach is not an ECM optimization method in itself, it indicates the direction in which ECMs should be tuned, since it calculates forecast error dependencies on ECMs. D08 also includes ODI estimation because it is an extension of Langland and Baker (2004) (LB04), which is an ODI estimation method involving the calculation of forecast error dependencies on observational data. Both of these ECM optimization methods therefore include ODI estimation.

This paper describes the development of ECM optimization and ODI estimation in the JMA global 4D-Var system.

2. ECM optimization and ODI estimation with DIC

DIC is an ECM optimization scheme that uses the theoretical relationships between ECMs and the cost function of 4D-Var as follows:

$$2J = N - TR(\mathbf{HK}) = N - DFS \qquad (1)$$

Here, $\mathbf{K}$ is the Kalman gain, $\mathbf{H}$ is a partial derivative of the observation operators, TR is a trace operator, N is the number of observation data, and J is the cost function of 4D-Var. This equation is valid for each block diagonal part of the observation ECM, defined as $\mathbf{R}$, and can be used to optimize $\mathbf{R}$ for each observation dataset. We implemented the DIC method on the JMA global 4D-Var system.

The results of DIC optimization show that diagonal components of the optimized $\mathbf{R}$ are about 30% of current settings for most of satellite radiance data, while are comparatively resemble the current settings for other conventional data. These results are consistent with departure value (observation minus guess) statistics, and the optimization recovers the theoretical relationships between cost functions and observation data numbers (Ishibashi, 2006). DIC includes ODI estimation as described in the introduction, since Equation (1) includes DFS. However, since this equation is correct only if DAS is optimal, DFS is shown after DIC optimization in Figure 1 (reproduced from Ishibashi, 2006). It can be seen that the contributions of radiance data and conventional data to analysis accuracy are about the same.

DIC enables determination of ECMs objectively rather than by trial and error. However, data assimilation cycle experiments with tuned ECMs using DIC (figures not shown) show that there are still several factors for consideration to improve analysis and forecast accuracy, including observation error correlation and the biases of the NWP model.

3. ECM optimization and ODI estimation with D08

D08 is a method used to calculate the dependencies of forecast errors on ECMs. It consists of three parts: the first is calculation of the forecast error sensitivity field (SF); the second is calculation of the dependencies of SF on observational data; the third is calculation of the dependencies of SF on ECMs. The first two parts are the same as the calculation of LB04, and the last one is a new addition in D08. This means that LB04 is included in the D08 approach.

LB04 is an ODI estimation method that calculates ODI as a forecast error reduction by assimilating observational data using adjoint operators of the forecast model and DAS. As the construction of an adjoint operator for DAS requires large changes to DAS, the implementation cost of LB04 is not small. We divide the adjoint operators of DAS into two-step linear problems and solve them using fixed original 4D-Var code (Tre'molet, 2008, TELLUS).

We evaluate the errors of a 15-hour forecast in terms of dry total energy (TE), and then calculate its sensitivity field (SF). To evaluate the validity of the calculated SF, we construct an approximate analysis error field from the SF through multiplication by a scalar coefficient, as a normalized SF is a good approximation of the analysis error field (Rabier, 1996, QJRMS). We then make an optimal initial field by extracting the approximate analysis error field from the original initial field. Figure 2 shows the error of the forecast from the optimal initial field and from the original initial field. As an explicit forecast error reduction can be seen from the optimal initial field, our SF calculation can be considered valid.

Figure 3 shows the results of LB04 using the SF. It indicates that the largest contributions to forecast error reduction are brought by AMSU-A sensors, with the next being radiosonde data in the JMA 4D-Var system. The contributions from the sum of all satellite radiance data and the sum of the remaining data (e.g., radiosondes and satellite winds) are compatible. However, comparing the results with those of ECMWF suggests that satellite contribution is rather small as hyper-spectral sounders (AIRS and IASI) and GPS data are not used (or are not enough used) in the JMA 4D-Var

system, and also because the **R** settings for radiance data are too large. We also check the effects of the norm form used in the forecast error specification. If we use wet TE, the water vapor channel contributions increase slightly (figures not shown).

To check the ability of LB04 to detect erroneous observation data, we implemented a very small observation error setting for Channel 8 of AMSU-A/METOP in 4D-Var. LB04 detects forecast error increases from this data (Figure 4).

Finally, we construct a D08 system by extending the LB04 system, and evaluate the dependencies of forecast error on the observation ECM, **R**. These calculations are given by the following equation:

$$\partial J/\partial R_{p,q} = \partial J/\partial y_p \sum_s R^{-1}_{q,s}\left(Hdx - d\right)_s . \quad (2)$$

Here, J is the forecast error in TE, p, q and s are indices for observational data, y is the observation value and dx is the analysis increment. Eventually, the calculation only multiplies the coefficients by the LB04 results. The results of D08 show that reduction of the observation error setting for most radiance data will reduce the level of forecast error (Figure 5). These results are consistent with those of the DIC approach described in Section 2. In fact, a 20-percent reduction of these observational data errors leads to the forecast error reduction shown in Figure 6.

4. Conclusions

Here we have reported on the development of ECM optimization and ODI estimation in the JMA global 4D-Var system. Further development and improvement of these methods, including measures such as the introduction of observation error correlations to DIC, are planned to reduce analysis and forecast errors in the future.

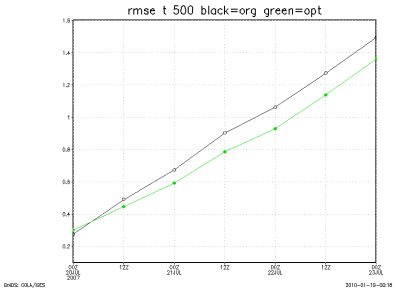

Figure 2. Root mean square error (RMSE) for 500-hPa temperature of forecasts from the original initial field (black line) and from the optimized initial field (green line)

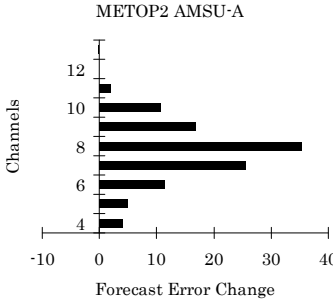

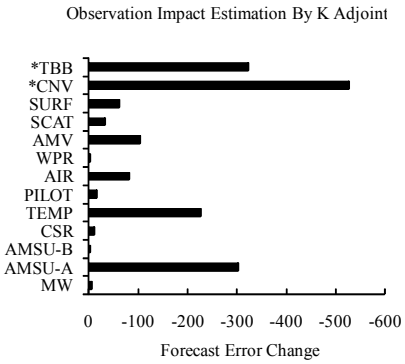

Figure 3. Results of LB04 ODI estimation in JMA's global 4D-Var DAS calculated for the initial, 00 UTC on July 20, 2007

Figure 5. Results of D08 – forecast error change (measured in total energy) caused by perturbing 1 (K) of observation error standard deviation in the JMA global 4D-Var system for AMSU-A/METOP2

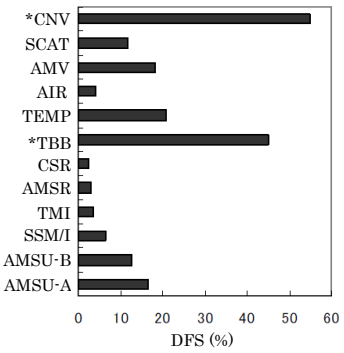

Figure 1. DFS (ratio to total DFS in %) for the JMA global 4D-Var system after DIC optimization. *TBB denotes all radiance data, *CNV denotes all data except *TBB, SCAT denotes QUIKSCAT, AIR denotes airplane, TEMP denotes radiosonde, CSR denotes geostationary satellite radiance, and the others denote individual satellite sensor names. This figure is adapted from Ishibashi (2006).

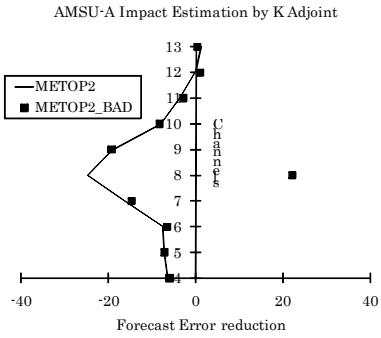

Figure 4. Example of erroneous channel detection by LB04. The solid black squares show the ODI estimation of LB04 for a case in which Channel 8 of AMSU-A/METOP2 is given an incorrectly small observation error setting. The solid line shows the case of routine setting for comparison.

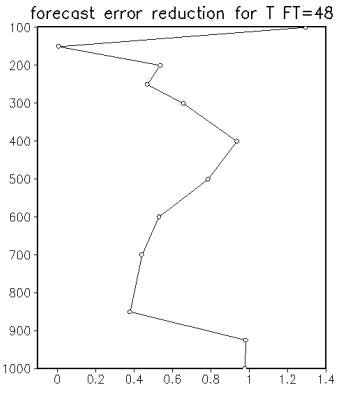

Figure 6. Forecast error reduction by **R** tuning according to the results of D08 estimation. The figure shows the global average of the normalized RMSE difference (routine setting minus tuned setting for temperature).

Data Assimilation of GPS Precipitable Water Vapor into the JMA Mesoscale Numerical Weather Prediction Model

Yoshihiro Ishikawa
Numerical Prediction Division, Japan Meteorological Agency
1-3-4 Otemachi, Chiyoda-ku, Tokyo 100-8122, Japan
E-mail: ishikawa@met.kishou.go.jp

1. Introduction

One of the most important objectives of mesoscale numerical weather prediction (NWP) is the precise identification of the timing and location of heavy rainfall, and NWP improvement is essential to enable quantitative forecasting of extreme precipitation with a lead time. The Japan Meteorological Agency (JMA) operates a mesoscale model (MSM) with a horizontal resolution of 5 km to forecast mesoscale events over the country's islands. The MSM operationally produces 15-hour forecasts four times a day (at 00, 06, 12 and 18 UTC initial times) and 33-hour forecasts four times a day (at 03, 09, 15 and 21 UTC initial times) to assist forecasters in issuing weather warnings. As a data assimilation system for the MSM, the nonhydrostatic mesoscale four-dimensional variational data assimilation system (JNoVA) was newly implemented in April 2009 in place of the hydrostatic Meso 4D-Var system.

Atmospheric delay in GPS (Global Positioning System) signals caused by precipitable water vapor (PWV) is one of the most important data types for improvement of MSM precipitation forecasts considering that moisture observations are insufficient compared with other meteorological variables. Since 1994, the Geographical Survey Institute (GSI) of Japan has deployed a nationwide ground GPS network called GEONET, which covers the entire Japanese archipelago and comprises more than 1,200 ground receivers a mean distance of 15 – 25 km apart (Figure 1). Although GPS data are primarily implemented for monitoring crustal deformation, they are also useful as water vapor sensors. Several studies have shown that water vapor information retrieved from GEONET has a positive impact on numerical weather prediction (NWP). JMA commenced operational use of GPS-derived PWV in NWP with JNoVA on October 28, 2009. Precipitation forecasting was improved by taking moisture information as an initial condition of the MSM.

2. Quality control

As Japan is characterized by steep mountainous terrain and MSM employs smoothed topography, large discrepancies exist between the GPS antenna height and the corresponding MSM surface height in mountainous areas. In order to adjust differences in the PWVs between the first guess and the GPS, the first guess PWV is interpolated or extrapolated from the model surface to the actual terrain surface as follows:

(1) If the model surface is higher than the actual terrain surface, the model PWV is extrapolated to the actual terrain surface by assuming that the specific humidity between the two surfaces is equal to that in the lowest model layer.

(2) If the model surface is lower than the actual terrain surface, the model water vapor between the two surfaces is subtracted from the model PWV.

Quality checking is mainly based on the presentable errors of the GPS PWV data. Observed GPS PWV data are discarded unless all of the following conditions are satisfied:

(1) The actual surface elevation is less than 500 m.

(2) The absolute value of the elevation difference between the model surface and the actual surface is less than 200 m.

(3) The observed GPS PWV is between 1 mm and 90 mm.

(4) The absolute value of the PWV departure is less than 8 mm from the first-guess value after height correction.

The horizontal grid spacing of the inner model of JNoVA is 15 km, but the spatial density of GEONET stations is higher than this in some places. In order to avoid over-fitting, GEONET station thinning is performed so that the spatial density of GPS observations becomes coarser than 30 km. Since JNoVA assimilates observational data with one-hour slots in a three-hour assimilation window, we evaluated the GPS-derived PWV for each clock hour.

3. Impacts of experiment

The experiment for the three-hourly forecast-analysis cycle was performed without and with GPS PWV data for the period 17 – 25 July 2006. During this period, 33-hour forecasts were made four times a day at 03, 09, 15 and 21 UTC.

Figure 2 shows the root mean square errors (RMSE) for the surface relative humidity of the 33-hour forecasts for the experimental period. The surface relative humidity errors for these forecasts taking GPS PWV to an initial condition are remarkably small.

Figure 3 shows that the GPS PWV has a significantly positive impact on precipitation forecasting. An improvement of the equitable threat score for the three-hour accumulated precipitation forecast is seen for moderate rain.

Figure 4 shows a case of heavy rain during the experimental period. Figures 4b and 4c show the forecast for three-hour accumulated precipitation amounts starting from analysis without and with GPS PWV, respectively. Figure 4a shows the corresponding observation for radar-raingauge analyzed precipitation. Without GPS PWV data, the amount shown in the precipitation forecast in the rainfall area of Japan's Yamaguchi Prefecture was much smaller than that of actual observation. With assimilation of GPS PWV (Fig. 4b), more precipitation is predicted and the precipitation pattern is closer to the results of observation.

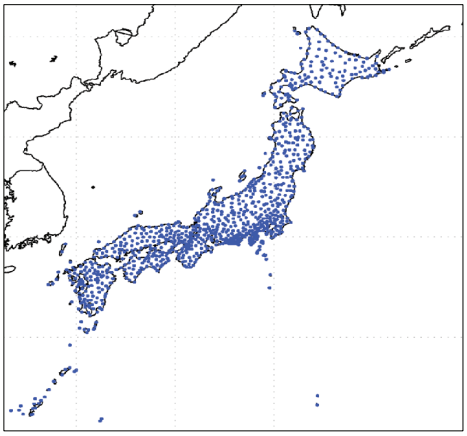

Fig. 1 Locations of GEONET sites over all the islands of Japan

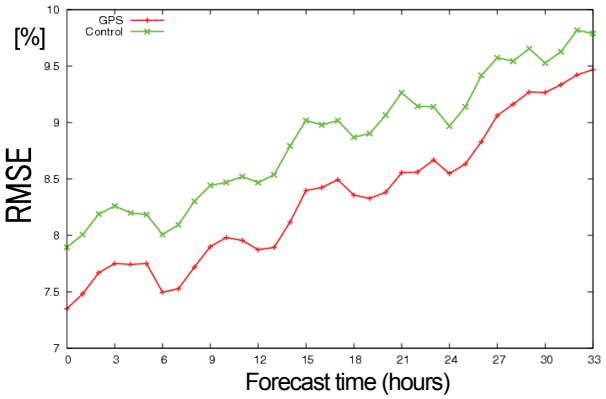

Fig. 2 RMSE of surface relative humidity for 33-hour forecasts for the period from 17 to 25 July 2006. This verification was used against hourly observations of relative humidity [%] by domestic SYNOP stations (at about 70 locations) and the calculated RMSE for observations in the forecast time. Forecasts starting from analysis with (red line) and without (green line) GPS PWV data are displayed.

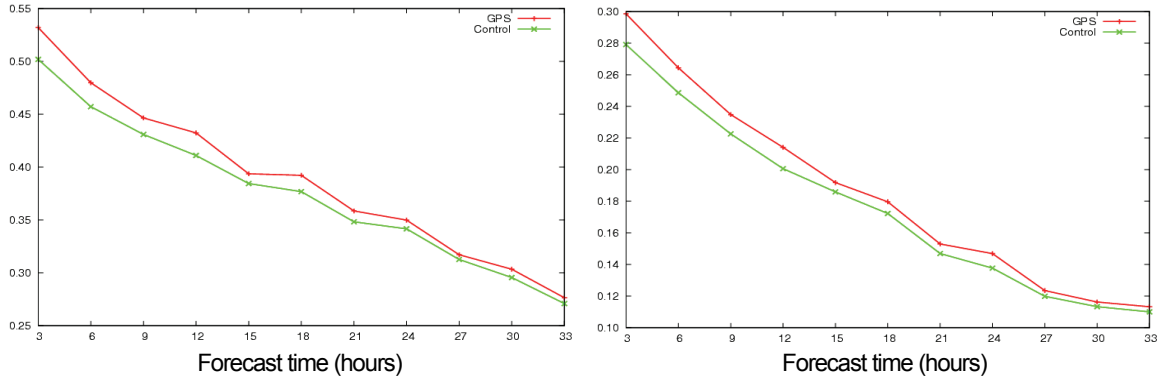

Fig. 3 Equitable threat score of 3-hour accumulated precipitation for 33-hour forecasts over Japan starting from analysis with (red lines) and without (green lines) GPS PWV data for the period from 17 to 25 July 2006. The threshold values are 1 mm (left) and 10 mm (right) with a verification grid distance of 10 km.

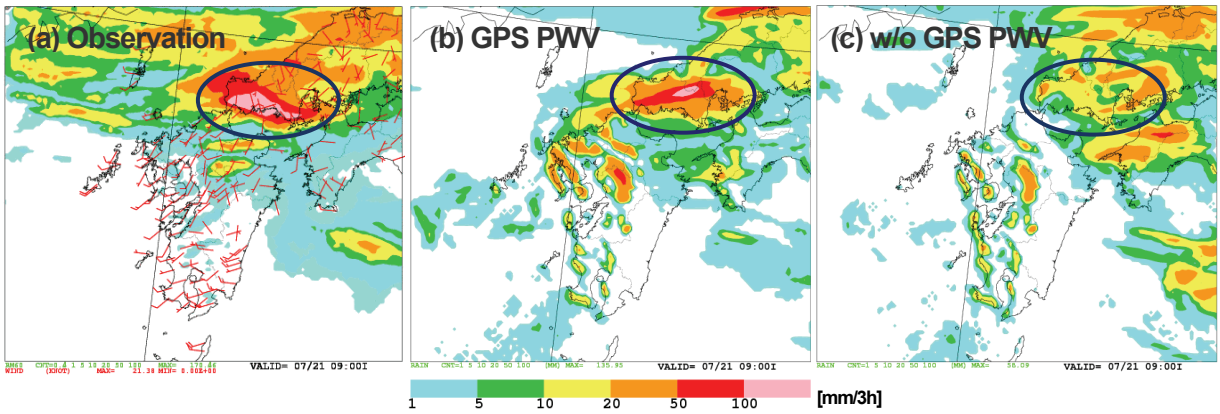

Fig. 4 Forecast FT = 00 – 03 and observations of three-hour precipitation amounts at an initial forecast time of 21 UTC on 20 July 2009. Left: radar-AMeDAS observations; center: forecast starting from analysis with GPS PWV; right: forecast starting from analysis without GPS PWV

The Use of Microwave Surface Sensitive Observations over Land and over Sea-Ice at Météo-France

Fatima Karbou, Florence Rabier, Elisabeth Gérard, Jean-Philippe Lafore, Jean-Luc Redelsperger, Olivier Bock

CNRM/GAME, Météo-France and CNRS
fatima.karbou@meteo.fr

Observations from AMSU-A & AMSU-B instruments provide relevant information about the vertical structure of the temperature and the humidity. However, the use of these observations in the context of data assimilation is still bellow requirements. In fact, AMSU observations which are sensitive to the surface are usually not assimilated because of large uncertainties about the surface temperature and emissivity (English 2007). Efforts have been undertaken at Météo-France in order to improve the representation of the surface at microwave frequencies. New methods for land emissivity and surface temperature modelling anchored on satellite microwave observations were tested. The methods, fully described in Karbou *et al.* (2006), were interfaced with the RTTOV model. (1) The first method is based on the use of averaged emissivity estimates calculated within the assimilation system two weeks prior to the assimilation period; (2) the second one uses a dynamically varying emissivity derived at each pixel using one surface channel or a selection of surface channels, and (3) finally the third method combines the two previous ones since it uses averaged emissivities and dynamically estimated skin temperature at each pixel using observations from one surface channel. The relevance of each of the three methods to assimilate microwave observations over land was investigated using AMSU-A, AMSU-B. The performance of the three methods were studied in terms of observation departures from first guess and from the analysis and also in terms of analysis and forecast impacts. The second method was found to be the most promising one for the French operational ARPEGE system and was operationally implemented in July 2008 (Karbou et al. 2010a).

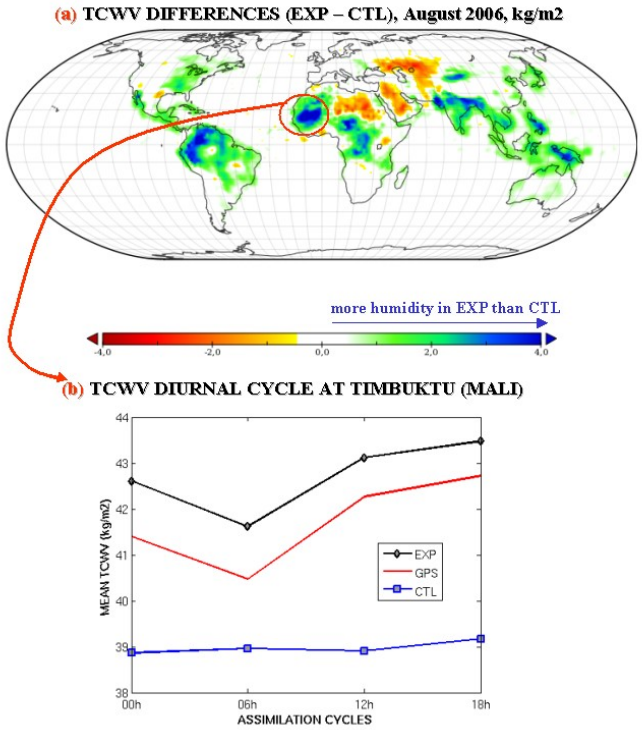

Figure 1 : (a) Mean TCWV analysis differences (experiment minus control) during August 2006. Negative (positive) values indicate that the control assimilation is more moist (dry) than the experiment. (b) Diurnal cycle of TCWV near TOMBOUKTOU estimated using GPS measurements and using analyses from CTL and from EXP assimilation experiments. Statistics are for 45 days (from 01/08/2006 to 14/09/2006)

Once the new land emissivity model implemented, strategies were explored to assimilate, for the first time ever, surface sensitive observations. Studies were undertaken to assimilate observations sensitive to the atmospheric boundary layer over land. In addition to a control experiment, a two-month experiment was run during the summer 2006. The latter assimilated low level temperature and humidity observations from AMSU over land. The assimilation of these observations impacts key parameters of the water cycle (Karbou et al. 2010b). An important change of the analyzed atmospheric fields and of the precipitation forecasts over the Tropics has been noted. Our experiment emphasizes the atmosphere moistening in India, South America and in West Africa together with a drying over Arabia and

North-East Africa (see Figure 1). The humidity change not only concerns the surface but also many levels of the atmosphere, up to 500 hPa. The humidity change was successfully evaluated using independent GPS data. The changes result in a better-organized African monsoon with a stronger ITCZ. Forecast errors were reduced over the Tropics leading to significant forecast improvements at higher latitudes at 48h and 72h ranges.

Over sea ice, the description of the emissivity is still unrealistic in the models (constant value of 0.99 for AMSU-B for instance). Consequently, almost no AMSU-A nor AMSU-B observations are assimilated over high latitudes. Bouchard et al. (2010) tested the surface emissivity model initially developed over land to improve the assimilation of AMSU observations over Antarctica and surrounding sea ice. The results were encouraging even though some residual biases were noticed over sea ice for AMSU-B observations. Since then, more in depth studies were undertaken to propose a new sea ice emissivity model suitable for microwave observations. The model is based on a direct retrieval of surface emissivity at one window channel (channel 3 for AMSU-A and channel 1 for AMSU-B). For AMSU-B observations, the sea ice emissivity model integrates a non linear frequency parameterization to describe the emissivity change from 89 GHz to 183 GHz. The performance of this model was examined : (a) many more AMSU observations are assimilated (b) RTTOV simulations are closer to the observations (see Figure 2) and (c) forecast skills are improved.

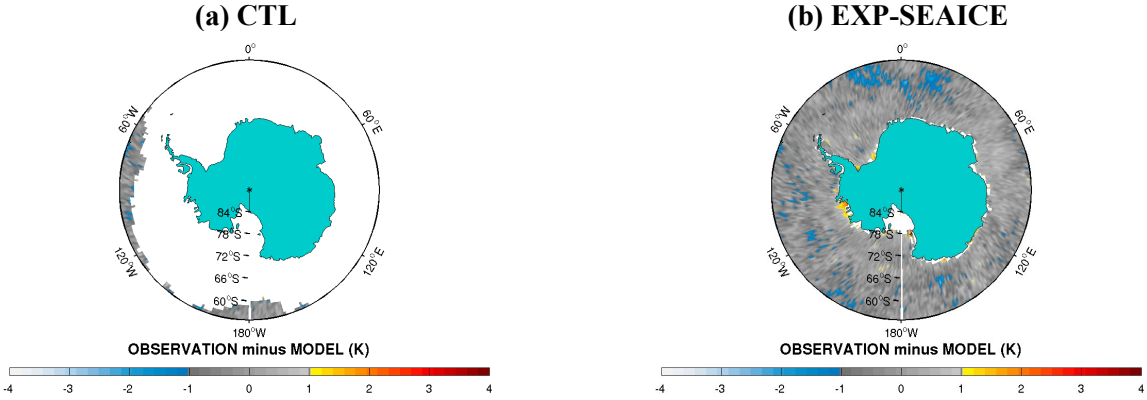

Figure 2 : Departures from First guess for assimilated AMSU-B channel 5 (183.31 ± 7.0 GHz) observations from (a) a CTL experiment and from (b) an experiment making use of a new sea ice emissivity model. Statistics are for 2 weeks (from 25/12/2008 to 06/01/2009)

REFERENCES

Bouchard, A., F. Rabier, V. Guidard, F. Karbou, 2010, Enhancement of satellite data assimilation over Antarctica, Monthly Weather Review, in press.

English, S., 2007: The importance of accurate skin temperature in assimilating radiances from satellite sounding instruments. IEEE Trans. On Geoscience and Remote sens., 46, 403–408.

Karbou, F., Gérard, É. and Rabier, F., 2006: Microwave land emissivity and skin temperature for AMSU-A and –B assimilation over land. *Q. J. R. Meteorol. Soc*., 132, 2333-2355

Karbou, F., E. Gérard, F. Rabier, 2010a, Global 4D-Var assimilation and forecast experiments using AMSU observations over land. Part-I: Impact of various land surface emissivity parameterizations, *Weather and Forecasting*, 25, 5–19.

Karbou, F., F. Rabier, J-P. Lafore, J-L. Redelsperger, O. Bock, 2010b, Global 4D-Var assimilation and forecast experiments using AMSU observations over land. Part II: Impact of assimilating surface sensitive channels on the African Monsoon during AMMA, *Weather and Forecasting*, 25, 20–36.

Impacts of Surface Pressure Observations in the Antarctica on JMA's Global Data Assimilation and Forecasting

Masahiro Kazumori and Hirokatsu Onoda
Numerical Prediction Division, Japan Meteorological Agency
E-mail: kazumori@met.kishou.go.jp, h.onoda@met.kishou.go.jp

Background

Part of JMA's work involves assimilating surface pressure observations in the global data assimilation system. Direct measurement of meteorological parameters, such as surface pressure through conventional observation instruments provides an important source of data for maintaining operational analysis and forecast accuracy. Antarctica is a data-sparse region whose land surface is characterized by extremely steep topography and is covered with snow and/or ice for most of the year. This land surface situation makes it difficult to use surface-sensitive satellite data in NWP because of the insufficient accuracy of the surface emissivity modeling in radiative transfer calculation. Accordingly, surface observations in Antarctica are considered more important than those in other areas, and JMA's system has accepted these observations as much as possible.

However, recent improvements to the horizontal resolution of JMA's global forecast model (to about 20 km) and analysis accuracy have revealed the improper use of surface pressure measurements in Antarctica within the current JMA system. As a result, this is an appropriate time to review quality control performance for surface observations in JMA's global data assimilation system.

In this study, we identified unacceptable surface pressure measurements in Antarctica for the global data assimilation system. As data rejection is difficult in the current normal quality control scheme, data which have systematic biases were blacklisted in the system. As a result, improvements in analysis and forecast were confirmed.

Surface pressure observation in Antarctica

Figure 1 shows the reported locations of surface pressure observations in Antarctica from 20 July to 9 October 2009. The data were assimilated after quality control in the operational system. Figure 2 shows time sequences of surface pressure innovations (O-B) for data at two locations. We found that surface observations at several points in Antarctica had large negative or positive biases against the background field for the period, and a large bias was also found for another period. A scheme to correct differences between the model topography and the reported topography was utilized in quality control. The remaining bias could be caused by a number of factors (e.g., disagreement between the reported altitude of observation location in the WMO station table and the actual instrument altitude, erroneous instrument characteristics, JMA global model biases). It should be noted that about 17% of surface observations in Antarctica were blacklisted. Other data at many locations showed good agreement with the background field for the same period.

Impact of data removal on JMA's operational data assimilation and forecasting

Figure 3 shows a comparison of the root mean square (RMS) for analysis increments of 500-hPa geopotential height with and without biased data. After the removal of biased surface pressure data at several locations in Antarctica, the erroneous analysis increment for 500 hPa disappeared. RMS errors for 24-hours forecasts against the analysis were also improved around Antarctica (Fig. 4). The biased data were blacklisted on December 10, 2009 in the operational system. Figure 5

shows a time sequence of monthly averaged RMSEs of 24-hour forecasts for 500-hPa geopotential height in the Southern Hemisphere. An improvement in operational JMA forecast accuracy was confirmed in comparison with other NWP center forecast scores in Dec. 2009.

Summary

In JMA's global data assimilation system, quality control for surface pressure data in Antarctica was revised on December 10, 2009. Although satellite data have a dominant impact on analysis and forecast accuracy, the removal of biased conventional data produced improvements in the operational forecast score. This outcome suggests that quality control for conventional data is more important than expected in the JMA system, especially for data-sparse areas.

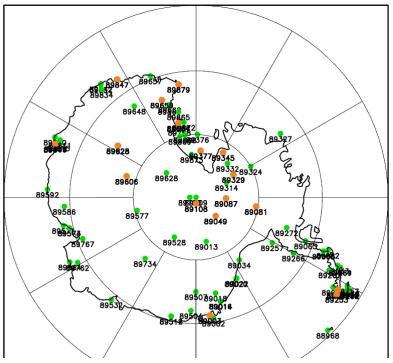

Fig. 1 Reported locations of surface pressure data in Antarctica. The orange points indicate blacklisted observation locations.

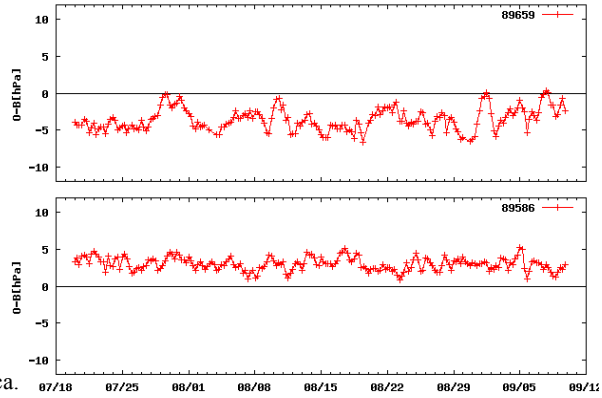

Fig. 2 Time sequences of surface pressure innovations (observed – background) for biased data against JMA background field in Antarctica.

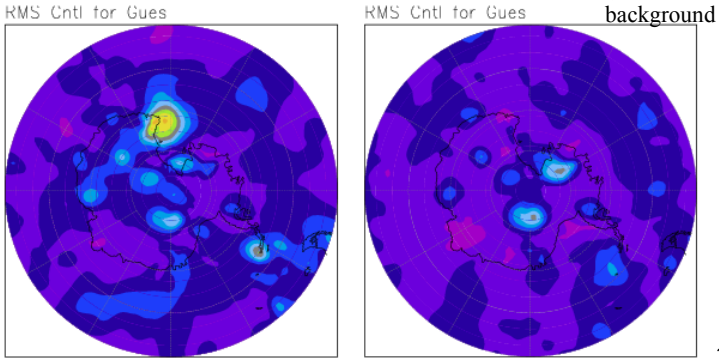

Fig. 3 Comparison of three-day averaged root mean squares for analysis increments of 500-hPa geopotential height. On the left are the RMSs before data removal (i.e., with biased surface pressure data), and on the right are those after data removal (without biased data).

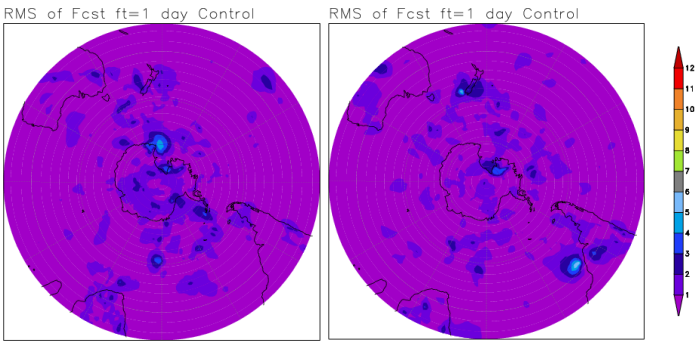

Fig. 4 Three-day averaged RMSEs of 24-hour forecasts for 500-hPa geopotential height. On the left are the RMSEs before data removal, and on the right are those after the data removal.

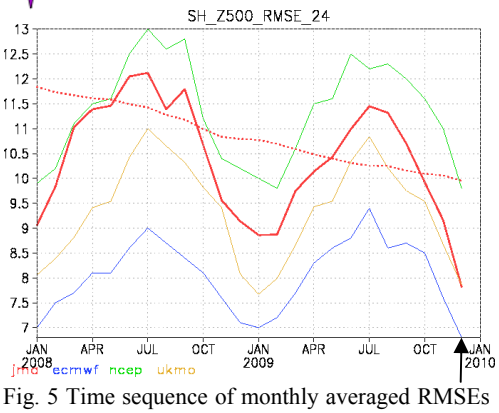

Fig. 5 Time sequence of monthly averaged RMSEs of 24-hour forecasts for 500-hPa geopotential height in the Southern Hemisphere for several NWP centers. The dotted line is the 12-month moving average. The black arrow indicates data for Dec. 2009

Initial Results of a Direct Radiance Assimilation Experiment in the JMA Mesoscale 4D-Var data assimilation system

Masahiro Kazumori
Numerical Prediction Division, Japan Meteorological Agency
E-mail: kazumori@met.kishou.go.jp

Background

JMA operates the Mesoscale Model (MSM) and the 4D-Var data assimilation system [1] to provide disaster prevention information for Japan and its surrounding areas. Various observational data (surface, ship, buoy, radiosonde observation, wind profiler, ground-based radar data (rain and wind), Total Precipitable Water (TPW) and rain rate from microwave imagers, temperature profiles from satellite sounding instruments, atmospheric motion vectors derived from MTSAT images and ground-based GPS TPW) are used in operational analysis. Remote sensing from polar-orbit/geostationary satellites is important in obtaining information on rapidly changing atmospheric states over a wide area.

Meanwhile, variational data assimilation schemes allow observations to be different from analysis variables, and direct radiance assimilations make observation errors easier to define and less correlated than retrievals. Direct radiance assimilation in JMA's global data assimilation system has shown large positive impacts on analysis and forecast since 2004. Accordingly, direct radiance assimilation in the MSM is expected to provide improvements in analysis and forecast. Additionally, raw-level satellite data (level 1b/1c brightness temperature) will generally become available sooner than retrieved data after the launch of a satellite. The direct use of radiance is therefore important not only for forecast improvement itself but also for the early utilization of satellite data, and is indispensable for the future use of cloud- and rain-affected radiance in the JMA system.

In this study, RTTOV-9 [2] was implemented as an observation operator for radiative transfer calculation in the JMA Mesoscale 4D-Var data assimilation system. This is the same radiative transfer model used in the JMA global 4D-Var analysis [3]. The initial study focused on the impacts of directly using AMSU-A radiances from the NOAA-series, Metop and Aqua satellites.

Experimental design

JMA performs MSM analysis eight times a day. Early provision of MSM forecast outputs for Japanese forecasters requires a short cut-off time for observational data reception to enable the start of analysis. The current cut-off time is 50 min. after the analysis time, so data directly received from Japanese local stations are suitable for this system. NOAA satellite, MTSAT and Aqua/AMSR-E data are currently available through direct reception in JMA. In the experiment, AMSU-A radiances of the NOAA series, Metop and Aqua were used instead of retrieved temperature profiles. The experimental results were compared with the current retrieval assimilation results. Other radiance data, such as moisture channels from MHS/AMSU-B, Clear Sky Radiance (CSR) from MTSAT and radiances from microwave imagers, were not used in either experiment. The operational cut-off time was applied for the AMSU-A data set to estimate the real impact in JMA's operational system. The data-thinning distance was set as 40 km (the MSM inner-model resolution is 15 km), and available AMSU-A tropospheric channels (channel 4 to 8) were selected for the assimilation. Higher peaking channels were not used due to the limitation of the model-top height in JMA's MSM (about 22 km). Atmospheric profiles over the model's top height were extrapolated with the temperature lapse rate of US standard atmospheric profiles for radiative transfer calculation. The bias correction and observation error assignment for brightness temperatures were the same as those for the JMA global analysis. The period from

July 7 to 26, 2009 was selected to study cases of heavy rain in Japan.

Results and summary

The results showed better fits to radiosonde observations (RAOB) for three-hour forecasts in terms of geopotential height, temperature and wind (Fig. 1). Although there was no significant impact on the forecast of precipitation amounts, some improved cases of rain forecasts associated with cold fronts were found (Fig. 2). The predicted location of the rainfall band showed good agreement with the observed rainfall location in the direct radiance assimilation. It is presumed that the direct radiance assimilation of temperature sounding brought realistic atmospheric stability in the analysis and forecast field, which led to the improved forecast location of the rainfall band. The direct radiance assimilation of temperature sounding data showed a moderate and indirect impact on precipitation. In order to produce a larger impact on moisture field and precipitation forecast, moisture sensitive channels from MHS/AMSU-B and CSR would need to be incorporated simultaneously. In this initial experiment, successful implementation of RTTOV-9 as the radiative transfer model into JMA's mesoscale analysis and the advantages of direct radiance assimilation over the retrievals were confirmed. To implement the operational use of various radiance data in the JMA system, further studies regarding the impact of radiance assimilation on moisture sensitive channels are planned.

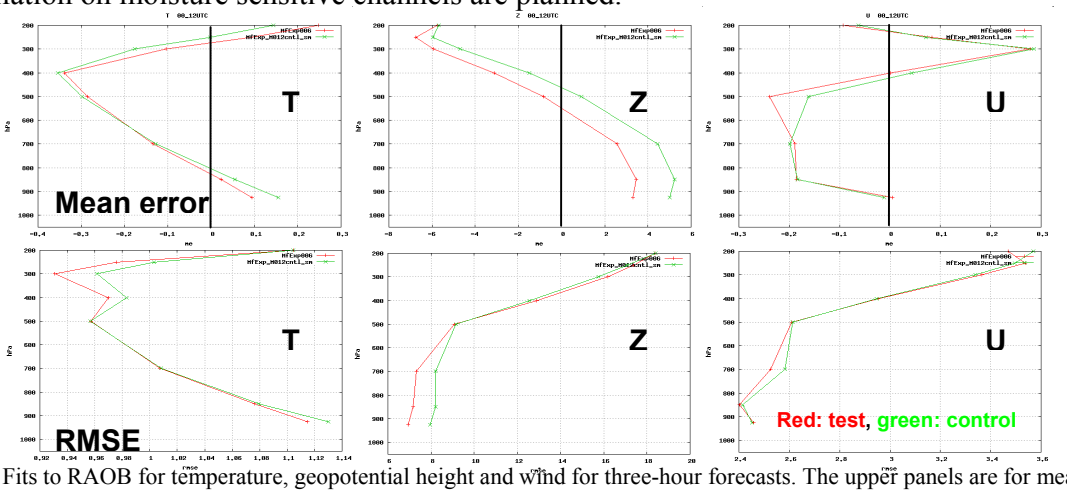

Fig. 1 Fits to RAOB for temperature, geopotential height and wind for three-hour forecasts. The upper panels are for mean errors, and the lower panels are for RMSE. The red lines show Test (radiance) and the green lines show Control (retrieval).

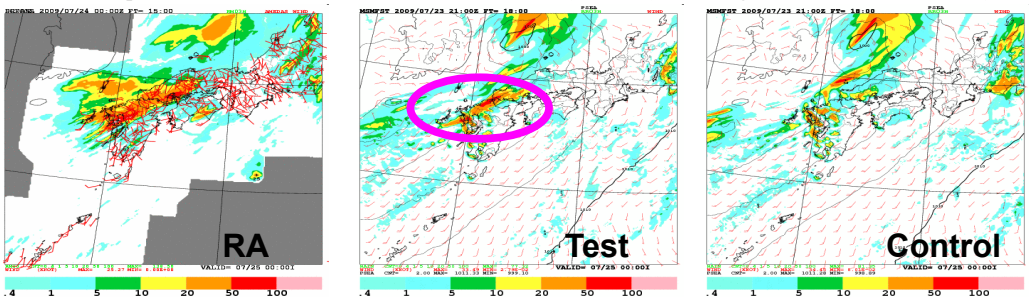

Fig. 2 Three-hourly accumulated precipitation of 18-hour forecasts from 23 Jul. 2009 at an initial time of 21 UTC. From the left, analyzed precipitation, the forecast of Test (radiance assimilation) and that of Control (retrieval assimilation) are shown.

References

[1] Honda, Y. and K. Sawada, 2009: "Upgrade of the Operational Mesoscale 4D-Var System at the Japan Meteorological Agency," *Res. Activ. Atmos. Oceanic Modell.,* 39, 1.11 – 1.12

[2] Saunders, R. W., 2008: *RTTOV-9 Science and Validation Report.* EUMETSAT, pp. 74

[3] Kazumori, M., 2009: "Impact study of a fast radiative transfer model, RTTOV-9, in the JMA global 4D-Var data assimilation system," *Res. Activ. Atmos. Oceanic Modell.,* 39, 1.21 – 1.22

Recent Modifications of Tropical Cyclone Bogus Data in the JMA Global Data Assimilation System

Yuki Kosaka (*1) and Akira Okagaki (*2)
(*1) Meteorological Satellite Center, Japan Meteorological Agency
E-mail: yuki-kosaka@met.kishou.go.jp
(*2) Numerical Prediction Division, Japan Meteorological Agency
E-mail: a-okagaki@met.kishou.go.jp

Introduction

In the JMA global data assimilation system, bogus data are generated and assimilated for tropical cyclones (referred to here as TCs) over the western North Pacific. Generally in areas mainly over the ocean, the number of observational data from around TCs is insufficient to allow the generation of an appropriate TC structure in an initial field. Bogus data are intended to represent accurate TC structure in initial fields and improve TC forecasting.

How bogus data are generated

Bogus data consist of surface pressure and winds around a TC. A typical TC structure is created using the central position, the central sea level pressure and a 15 m/s wind speed radius, which are analyzed by forecasters.

The TC structure is created as follows: First, the axisymmetric surface pressure is calculated using Fujita's formula (Fujita, 1952). Then, upper wind data are also produced using an empirical formula based on Frank's statistical analysis (Frank, 1977). Finally, the asymmetric component is derived from the first guess field and added to the axisymmetric structure.

The bogus data are produced from observation of this structure, and are simultaneously assimilated with other observational data. Until March 2009, bogus data in operational global analysis were distributed as shown in Figure 1.

Modification of horizontal distribution

Bogus data located in the vicinity of a TC's center seem to have a relatively higher level of quality than those far from it because they are based on analysis by forecasters, while those farther away are estimated using an empirical formula.

Figure 2 shows the modified distribution of bogus data; it can be seen that more are near the TC center, with fewer farther away. An experiment was performed using the JMA operational global data assimilation system to examine the impact of this change. The experimental period was from September 1 to 30 2008; forecasts were produced from each 12 UTC initial for the test run, while the control run employed original distribution (Figure 1). Figure 3 shows the forecast for Typhoon Sinlaku (T0813) from the initial time of 12 UTC on 9 September, 2008, as a case in which the test run improves on the TC forecast. From the initial field study, it is considered that this improvement was brought about by the reduced number of bogus data far from the center. Figure 4 shows statistical verification of the TC central position error. The test run reduces this error especially for longer-range forecasting as a result of the change. This modification was implemented in operational JMA global analysis in March 2009.

Re-modification

In 2009, it was found by assimilating bogus data for modified distribution that those located 50 km from the TC center tended to cause serious errors in analysis fields for some typhoons. When a TC significantly develops, the horizontal gradient of the physical fields (e,g,, sea level pressure, vorticity) may become steep in the vicinity of the TC center. In such cases, the difference between bogus data and the first guess near the center often has a much steeper gradient than the characteristic scale of increment in data assimilation, and this results in unrealistic deformation of the initial fields. In October 2009, the distribution of bogus data was re-modified as shown in Figure 5 to avoid unrealistic deformation near the TC center.

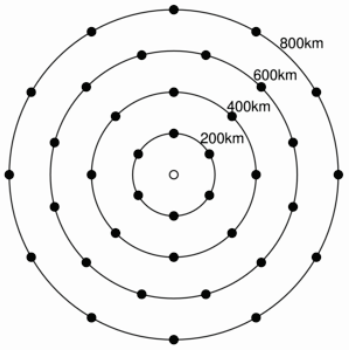

Figure 1. Horizontal distribution of TC bogus data. The white circle is the TC center, which has only surface pressure bogus data. The black dots have surface pressure data for the surface and wind data for upper levels (up to 300 hPa).

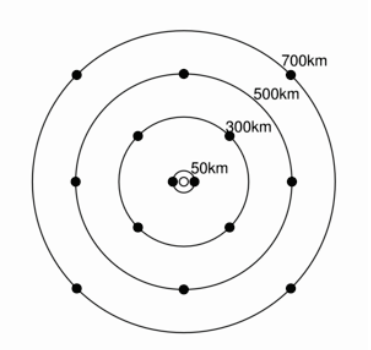

Figure 2. As per Figure 1, but with more data near the TC center and fewer farther away.

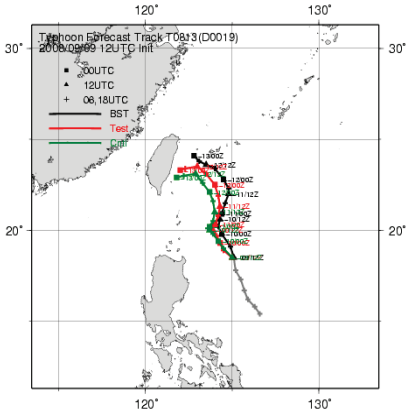

Figure 3. TC track forecast improvement resulting from changed bogus data distribution. The green line is the control, the red line is the test, and the black line is the best track.

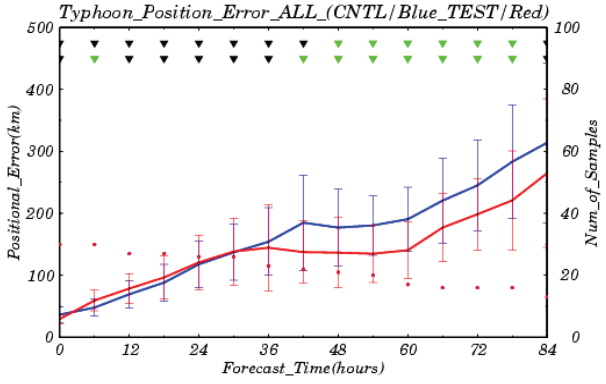

Figure 4. Statistics of TC central position error against forecast time. The blue line is the control, and the red one is the test.

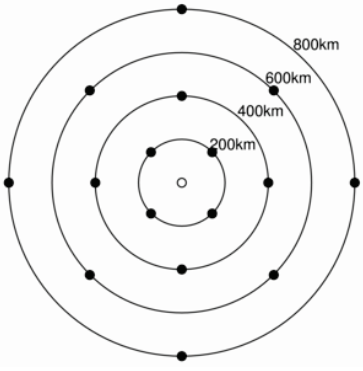

Figure 5. Distribution of TC bogus data as used in operational global analysis since October 2009

References

Fujita, T. 1952: Pressure Distribution within Typhoon. *Geophys. Mag.*, **23**, 437–451.

Frank, W. M. 1977: The structure and energetic of the tropical cyclone I. Storm structure. *Mon. Wea. Rev.*, **105**, 1119–1135.

Mesoscale LETKF Data Assimilation on Cyclone Nargis

Tohru KURODA, Kazuo SAITO, Masaru KUNII and Hiromu SEKO

Meteorological Research Institute, Tsukuba, Ibaraki 305-0052, Japan; tkuroda@mri-jma.go.jp

Nargis was a severe tropical cyclonic formed on 27 April 2008 in the Bay of Bengal, and made landfall on 2 May in southwestern part of Myanmar. Nargis caused a destructive storm surge over the Irrawaddy Delta, claiming more than one hundred thousand lives. If an appropriate warning was issued about 2 days before the landfall, the number of casualties might have been reduced.

JMA global analysis (horizontal resolution is about 20 km) and forecast data of GSM (horizontal resolution is about 50 km and valid time is every 6 hours) expressed Nargis' track to some degree, but the expression on the development was inadequate both in early and mature stages. Thus, it was difficult to foresee a severe storm from these data.

Recently, a downscale NWP using JMA nonhydrostatic model (NHM) and the JMA data was conducted in order to perform a forecast experiment of Nargis (Kuroda et al. 2010). They carried out a regional forecast with NHM, using the JMA global analysis as the initial condition and the GSM global forecast as the boundary condition. They also used the JMA global land surface analysis and JMA global SST analysis. NHM was executed with a horizontal resolution of 10 km for a square region of 3400 km around the Bay of Bengal. The initial time was set to 12 UTC 30 April, 2008. JMA analysis expressed Nargis as a weak depression of 999 hPa at that time, although the intensity was less than 985 hPa in the best track. After 42 hour (06 UTC on 2 May), NHM intensified the weak depression to a cyclone of 974 hPa, and predicted the landfall of the cyclone in southern Myanmar. The development predicted by NHM was much better than the GSM forecast (994 hPa; Fig. 1), but the intensity was still weaker than that of best track. A reason for the inadequate deepening in the NHM forecast may be a weak expression of the initial condition obtained from the JMA global analysis. It is necessary to correct the analysis in order to obtain a better initial field, using data assimilation.

A local ensemble transform Kalman filter (LETKF) is a new assimilation method based on the ensemble forecast. Miyoshi and Aranami (2006) applied this method to NHM (NHM-LETKF), and performed a preliminary data assimilation experiment.

We apply NHM-LETKF to the Nargis' case with data assimilation cycles depicted in Fig. 2. To obtain the analysis at 12 UTC on 30 April, the first cycle begins at 12 UTC on 28 April. The initial seed consists of 20 (or 40) JMA global analyses before 12 UTC 30 April. Then, a 6-hourly ensemble forecast with a 40km resolution is conducted using the seed as the initial values. The forecast result and observation data are assimilated with LETKF and resultant analysis ensemble are used as the initial values for the next 6-houly forecast. After iterating these steps, an analysis ensemble at 12 UTC on 30 April is obtained. The ensemble mean is used as an initial value for the extended forecast with a 10km resolution.

Selection of observation data is important since it affects the accuracy of the analysis. Observation data used in the JMA analysis are stored in a dataset called CDA4, and each of them has a quality control (QC) flag. Among the observation, sea surface winds observed by QuikSCAT are important since the data express a circulation of the cyclone (Fig. 3a). Since QC is based on global forecast model, some data have been rejected in the global analysis (Fig. 3b). QC for mesoscale system may be able to utilize such rejected data. .

Using the above design, we conducted preliminary experiments. Two kinds of observation dataset are compared; one the same as used in the JMA operational global analysis (GAQC), and another that included both GAQC data and sea surface winds rejected in QC (ALLSCAT). Extended forecasts for these cases did not show the sufficient intensification at both in initial and landfall stages, but the tracks expressed an encouraging result showing favorably suppressed northward deviation at landfall seen in the downscale experiment by Kuroda et al (2010) (Fig. 4). We will continue to perform more experiments and to investigate the influence of several components (e.g., QC criteria, initial seed, lateral boundary perturbations) on the analysis for the purpose of improving the forecast.

References

Kuroda, T., K. Saito, M. Kunii and N. Kohno, 2010: Numerical simulations of Myanmar cyclone Nargis and the associated storm surge Part I: Forecast experiment with a nonhydrostatic model and simulation of storm surge. *J. Meteor. Soc. Japan*, **88**. (in press)

Miyoshi, T., and K. Aranami, 2006: Applying a Four-dimensional Local Ensemble Transform Kalman Filter (4D-LETKF) to the JMA Nonhydrostatic Model (NHM). *SOLA*, **2**, 128-131.

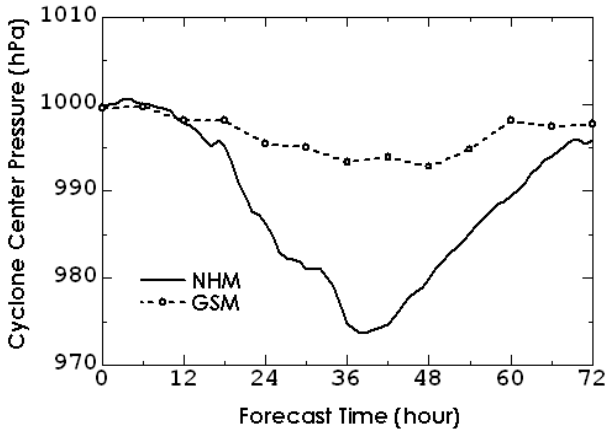

Fig. 1. Time evolution of sea level center pressure of Nargis by NHM and GSM forecasts. The initial time is 12 UTC 30 April 2008.

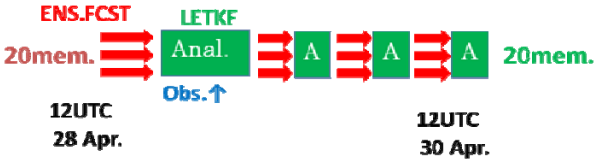

Fig. 2. Data Assimilation Cycles.

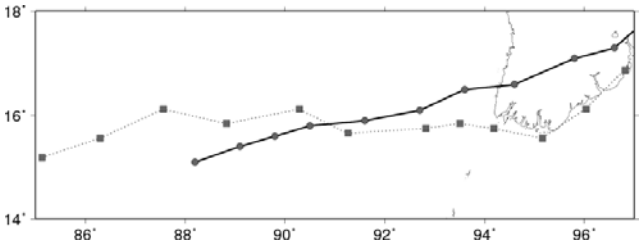

Fig. 4. Forecasted cyclone tracks around the Myanmar Delta. Thick solid line indicates the downscale experiment, and thin dotted line represents a extended forecast using LETKF result for the case of ALLSCATT with the ensemble size of 20..

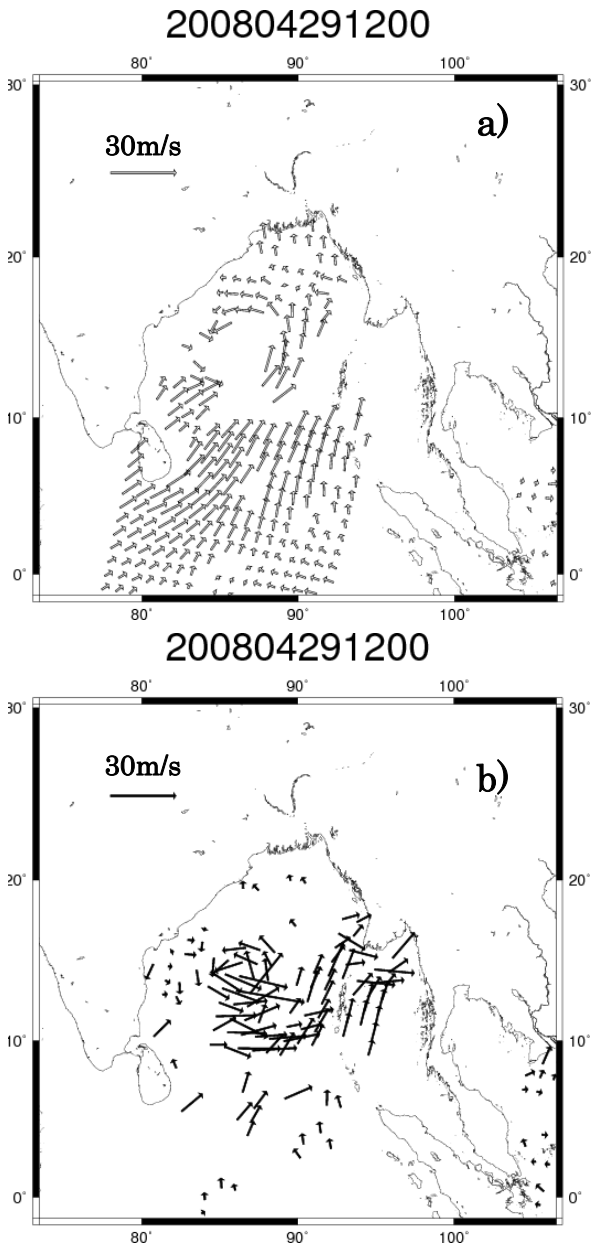

Fig. 3. Surface wind distribution at around 12 UTC on 29 April in the Bay of Bengal. a).Winds used in JMA global analysis. b) Winds rejected in QC.

Status of ATOVS Radiance Data Utilization in the JMA Global Data Assimilation System

Hidehiko MURATA
Numerical Prediction Division, Japan Meteorological Agency
1-3-4 Otemachi, Chiyoda-ku, Tokyo 100-8122, Japan
E-mail: hmurata@naps.kishou.go.jp

JMA assimilates ATOVS (AMSU-A, AMSU-B and MHS) radiance data in the operational JMA 4D-Var global data assimilation system. The satellites used in the system are shown in Table 1.

Since 9 December 2009, AMSU-A and MHS data from NOAA-19, which was launched on 6 February 2009, have been included in the system. The total number of assimilated ATOVS data has seen a modest increase of 5%, because the orbit of NOAA-19 is overlaps with that of NOAA-18. The improvement rate (%) in the RMSE of forecasting with assimilated NOAA-19 data is shown in Figure 1, which indicates a slightly positive impact in the Southern Hemisphere on the latter part of the forecast time.

NOAA-19 data from RARS[1] (A-P RARS[2] and EARS[3]) have also become available in addition to data from NOAA/NESDIS (Figure 2). These RARS data fill the gap in the NOAA/NESDIS data.

JMA set up a website for quality monitoring of the satellite data (radiance and atmospheric motion vectors) assimilated in the system. It shows sequences of statistics such as data counts, means and standard deviations of observation minus background (O-B) and observation minus analysis (O-A). The site can be accessed at
http://qc.kishou.go.jp/Sat_monit/seqgraph_radiance.html.

Table 1 ATOVS sensors used in the JMA global data assimilation system (as of Jan 2010)

Satellite	AMSU-A	AMSU-B or MHS
NOAA-15	Assimilated	Assimilated
NOAA-16	Assimilated	[4]Not assimilated (30 Apr 2009)
Aqua	Assimilated	
NOAA-17		Assimilated
NOAA-18	Assimilated	Assimilated
Metop-A	Assimilated	Assimilated
NOAA-19	Assimilated (since 9 Dec 2009)	Assimilated (since 9 Dec 2009)

[1] Regional ATOVS Retransmission Service
[2] Asia-Pacific RARS
[3] EUMETSAT Advanced Retransmission Service
[4] JMA stopped using NOAA-16/AMSU-B on 30 April 2009 due to an increase in sensor noise.

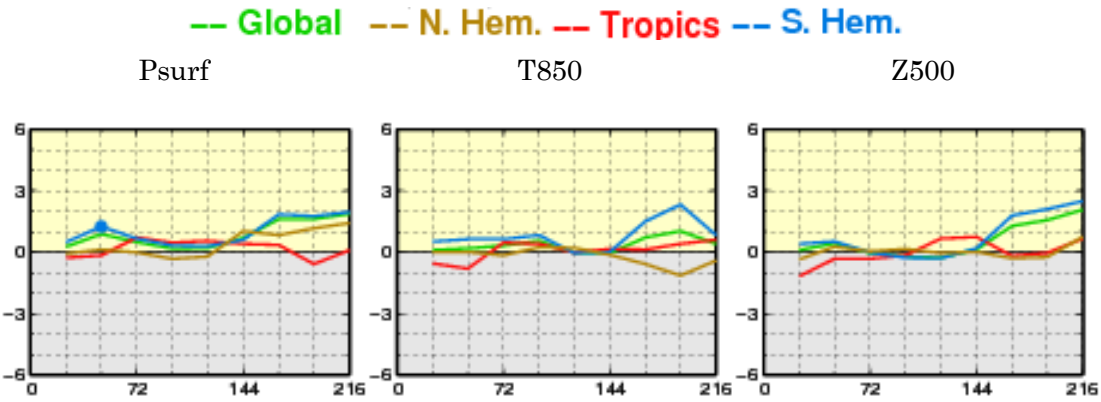

Figure 1: Rate of improvement (%) in the RMSE of forecasting with NOAA-19 data against that without for surface pressure (left), T850 (middle) and Z500 (right) in August 2009. The horizontal axis represents forecast hours. Lines in the upper (yellow) area indicate improved scores. Dots on the score lines represent statistical significance.

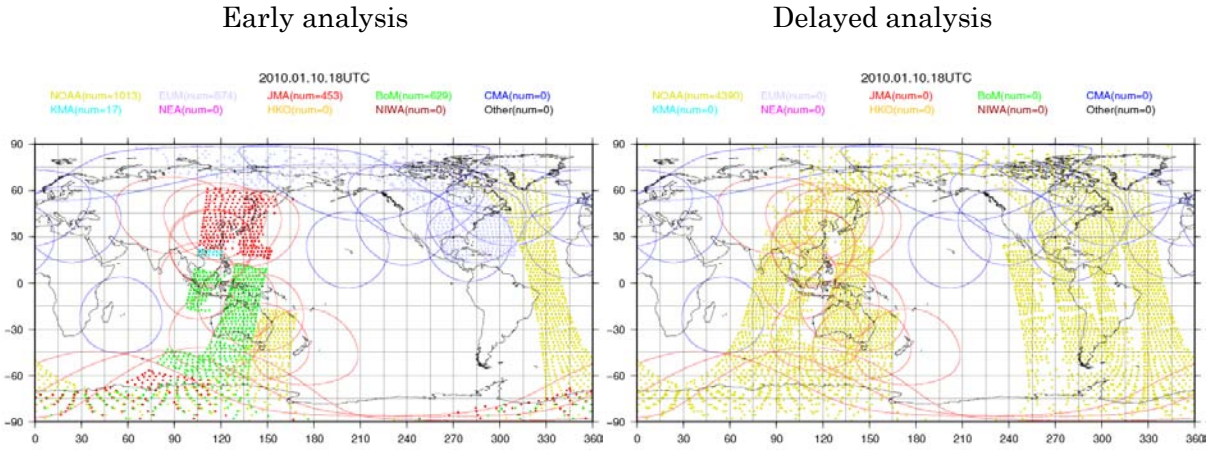

Figure 2: Snapshot of NOAA-19/AMSU-A data cover in the six-hour data assimilation window (at 18 UTC, 4 January 2009)

Left: early analysis with a 2.5-h data cutoff time from the analysis time. Right: delayed analysis (for generation of the first guess in the assimilation system) with a 6-h data cutoff time from the analysis time. The red circles are direct readout areas of A-P RARS stations, and the blue circles are those of EARS. The yellow plot points show data from NOAA/NESDIS, and points in other colors are from A-P RARS (red: JMA; sky blue: KMA; green: BoM) and EARS (light purple). The RARS data fill the gap in the NOAA/NESDIS data in the early analysis.

Resumption of Indian Radiosonde Temperature Data Usage in the JMA Data Assimilation System

Hirokatsu Onoda
Numerical Prediction Division, Japan Meteorological Agency
1-3-4 Otemachi, Chiyoda-ku, Tokyo 100-8122, Japan
(E-mail: h.onoda@met.kishou.go.jp)

1. Abstract

At the Japan Meteorological Agency (JMA), temperature data from Indian radiosondes have been blacklisted for many years due to low data quality. However, sequential updates to this radiosonde equipment since around spring 2009 have resulted in improved data quality at stations using the updated instruments. With careful monitoring and evaluation, JMA has decided to restart the use of these data in its data assimilation system.

2. Details of removal from the blacklist

We have sequentially monitored the mean error (ME) and standard deviation (SD) of temperature calculated against the JMA Global Spectral Model to identify stations with improved temperature data quality. At the point of WMO station ID 43333, for example, Hovmöller improvements for the ME and SD of temperature were seen around March 2009 (Fig. 1). Although small errors remain in the upper air, these may be due to model error and can be tolerated. We also found other improved stations with levels of data quality acceptable for operational use. Some stations require temperature bias correction because their departures (observation minus first guess field) are still large for some altitudes. The magnitude of bias correction is estimated from statistics on departures for sufficient periods.

In November 2009, some of the improved stations were removed from the blacklist and their data were re-assimilated into the JMA system. Figure 2 shows a map indicating the current usage status of Indian radiosondes. The red points indicate usage, the green points show usage with bias correction, and the blue points show stations not yet used.

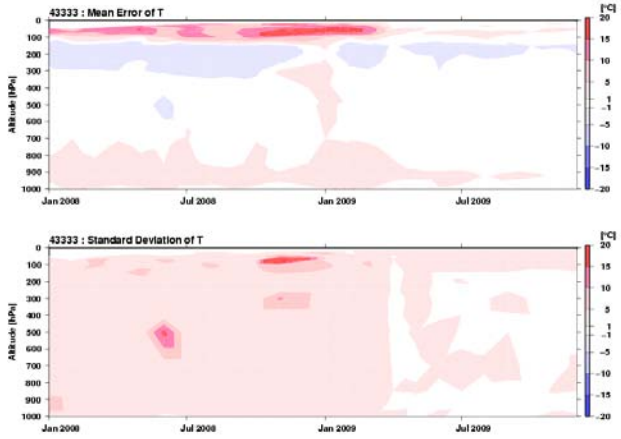

Fig. 1 Time sequences of ME and SD for temperature from January 2008 to December 2009 at station ID 43333 (11.7°N, 92.7°E)

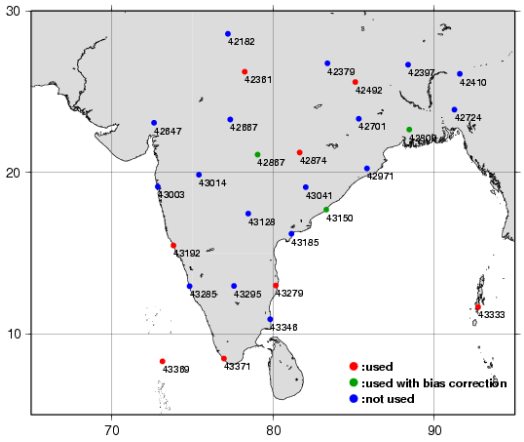

Fig. 2 Map showing current usage status of Indian radiosondes in the JMA data assimilation system

Assimilation of Metop-A and GRACE-A GPS-RO data for JMA's GSM

Eiji OZAWA, Yoshiaki SATO

Numerical Prediction Division, Japan Meteorological Agency

E-mail: e-ozawa@naps.kishou.go.jp, saty@naps.kishou.go.jp

1 Introduction

The Japan Meteorological Agency (JMA) started the assimilation of Global Positioning System (GPS) Radio Occultation (RO) data on November 30, 2009 for its operational global model. The assimilated data are obtained from Metop-A/GRAS through the GTS, and GRACE-A/BlackJack data are received via the Internet (Wickert et al., 2005).

2 Methods

We assimilate refractivity instead of bending angle to save on computational cost, and limited data for altitudes from 7 km to 30 km are assimilated. As refractivity data have a bias against the first guess in the troposphere and lower stratosphere, a bias correction procedure is implemented based on a linear regression approach. The regression coefficients are estimated using a Kalman filter for each analysis. The predictors for the bias correction are latitude, height and refractivity; Figure 1 shows that of a cross section of observation innovation (O-B), and Fig. 2 shows that of observation innovation (O-B) after bias correction. Observation errors and bias correction coefficients were defined in five latitudinal bands (90 – 60°S, 60 – 20°S, 20°S – 20°N, 20 – 60°N and 60 – 90°N) independently, and observation errors were defined as a function of height.

3 Assimilation experiments in the low-resolution model

Observation system experiments for GPS refractivity data were conducted for the periods of September 2008 and January 2009 to assess the impact of GPS refractivity assimilation. The control experiment (CNTL) had the same configuration as the operational global model, and GPS-RO data were added in the test experiment (TEST). Figures 3 and 4 show the differences (CNTL-TEST) in the RMS errors of 72-hour temperature forecasting at 50 hPa against their own initial fields. Positive values indicate that the RMS error in TEST is smaller than that in CNTL. In the Southern Hemisphere of the September experiment and in the Northern Hemisphere of the January experiment, red areas are dominant relative to blue areas. As the mean TEST RMS errors are smaller than those for CNTL, it can be concluded that GPS-RO data assimilation had a positive impact.

4 Summary

As GPS RO data contain systematic biases against the first guess of JMA's global model, bias-corrected GPS-RO data were assimilated in the experiments. As improvement of the analysis field was confirmed, JMA started to use Metop-A and GRACE-A GPS-RO data on November 30, 2009 in actual operation.

4 Acknowledgements

We would like to thank GFZ for providing GRACE-A/BlackJack data and EUMETSAT for providing Metop-A/GRAS data.

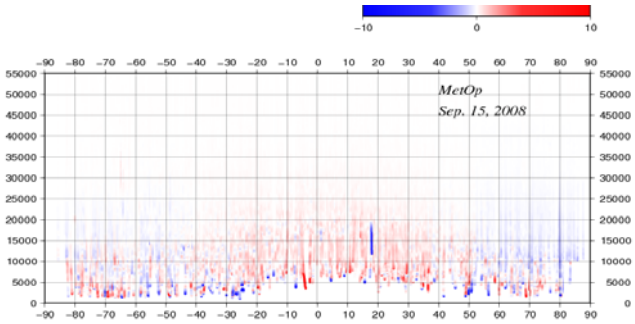

Fig. 1: Cross section of observation innovation (O-B) before bias correction. The vertical axis shows altitude (m), and the horizontal axis represents latitude as of September 15, 2008.

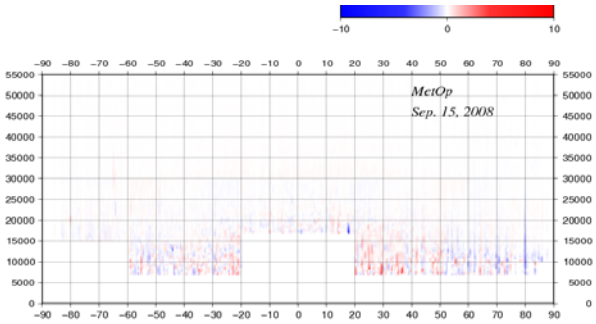

Fig. 2: Cross section of observation innovation (O-B) after bias correction and QC. Data for heights from 7 km to 30 km are used

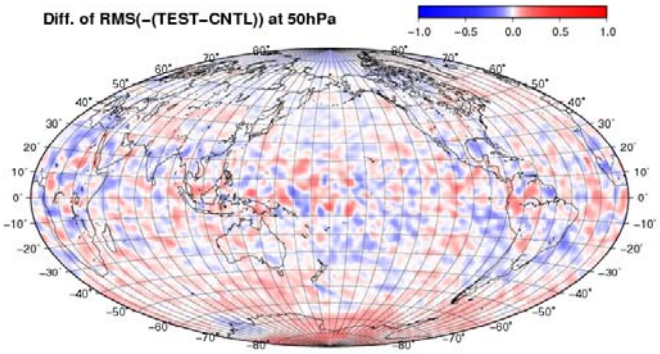

Fig. 3: Distribution map for 50-hPa RMS forecast error differences (CNTL-TEST) of temperature against the initial fields for the September experiment at FT = 72. Red areas represent improvement, and blue ones indicate deterioration.

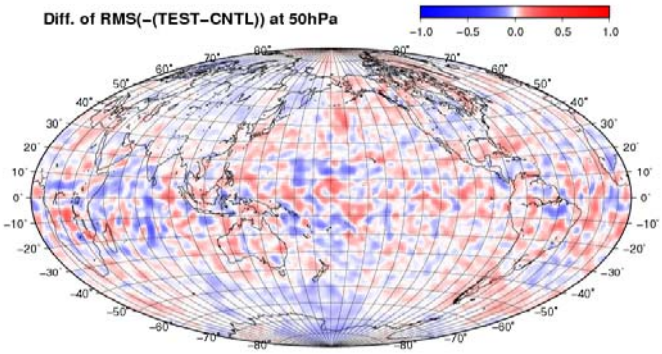

Fig. 4: As per Fig. 3, but for the January experiment.

References

Wickert, J., G. Beyerle, R. König, S. Heise, L. Grunwaldt, G. Michalak, C. Reigber, T. Schmidt, 2005: GPS radio occultation with CHAMP and GRACE: A first look at a new and promising satellite configuration for global atmospheric sounding. *Annales Geophysicae*, **23**, *3*, pp. 653-658.

Developments in the context of the Concordiasi project over Antarctica

Florence Rabier, Aurélie Bouchard*, Vincent Guidard

CNRM-GAME, Météo-France and CNRS (* and CNES)
42 Av Coriolis, 31057 Toulouse, France
florence.rabier@meteo.fr

Antarctica is operationally and climatologically data sparse, due to highly limited surface observing facilities in the high southern latitudes. Satellite measurements have the potential to fill these data gaps, but they present their own unique challenges and difficulties. This is true in particular of the data provided by hyperspectral infra-red sounders such as IASI. These challenges must be overcome and errors need to be reduced to produce accurate reanalyses for climate studies that are based primarily on observed conditions.

To improve our understanding of these challenges, a field experiment was organised over Antarctica (Concordiasi, Rabier et al, 2010), and in particular over the Concordia station. It must be noted that the atmospheric temperature profiles over the area exhibit a very strong inversion at the surface, with surface temperatures colder by up to 20K than the lower troposphere, which is indeed both difficult to model and to observe. The humidity is also quite low over inland Antarctica. During the Concordiasi field campaign, special measurements were obtained measuring the atmospheric profiles together with surface parameters, synchronised with the track of the European MetOp platform with the hyperspectral IASI sensor onboard. They were then compared to IASI measurements and to the outputs of the meteorological model of Meteo-France, especially adjusted for this area (Bouchard et al, 2010). The available in-situ observations obtained at Concordia were also compared to the results of IASI data retrievals using the Met Office 1D-VAR, part of the EUMETSAT NWP SAF. It was found that the problem of correct estimation of the surface temperature was the main limiting factor in the quality of IASI retrievals. A good prior estimation of skin temperature can be estimated using the radiative transfer equation together with IASI observations. In this study, the 943.25 cm^{-1} channel has been chosen for the estimation. This window channel has a very high transmittance. The skin temperature is calculated assuming a fixed surface emissivity of 0.99. Results are presented in Figure 1. In this figure, the skin temperature retrieved from the IASI window channel (blue line) is closer to the radiosounding surface temperature (black line) than the model skin temperature (red line), in terms of magnitude and time evolution. Based on this new estimation of the skin temperature, retrievals have been performed over 44 cases during Austral spring 2008. The root mean square (rms) between analysis and radiosounding, averaged on a layer of the troposphere between 250hPa and 650hPa, has been calculated for the temperature profile. The rms has decreased of about 10% from the case with skin temperature from model (rms about 1.18K) to the one with skin temperature from IASI window channel (rms of about 1.06K). To conclude, these additional data at the Concordia station have been used to improve our use of IASI data over the region. Results have shown that special attention has to be paid to the surface temperature estimation prior to the retrieval. Other sensitivity studies are under way to understand the impact of other parameters such as bias correction and error statistics. This study has highlighted the potential of IASI observations to contribute to a monitoring of weather and climate over the polar areas.

The second part of the project is a long-duration balloon campaign that will take place above Antarctica from September 2010 to early 2011. During this campaign, 18 12-m diameter superpressure balloons will be released in the stratospheric polar vortex from McMurdo station by the French space agency (CNES) in September and October. The balloons will fly around 20 km and will carry up to 60 kg of instrumentation and flight devices. It is expected that most of the balloons will be flying simultaneously for a few months in the austral spring and early summer and provide continuous observations of the polar atmosphere during that period.All balloons will carry a small in-situ meteorological package that will measure temperature and pressure. The horizontal wind at the flight level will be monitored from the successive GPS positions of the balloons. These observations will be sent in near real time to the GTS, so as to be assimilated in the NWP systems operated by the various meteorological services around the world, and thus contribute to the improvement of meteorological forecasts. 12 balloons will furthermore carry the driftsonde gondolas developed at NCAR. Each driftsonde gondola contains about 50 miniaturized dropsondes, which can be released individually on demand during the stratospheric balloon flight to provide high-resolution profiles of thermo-dynamic variables below the balloon. During the campaign, the dropsoundings will be mainly phased with the METOP passage above the balloons, in order to provide an

in-situ measurement that can be compared with the temperature profile retrieved from IASI observations. Some will also be deployed in the so-called "sensitive regions" of numerical forecasts, where small improvements in the description of the atmospheric flow can lead to large improvements in the simulation.

REFERENCES :
Bouchard A., Rabier F., Guidard V., Karbou F., 'Enhancements of satellite data assimilation over Antarctica'; Monthly Weather Review, 2010.

Rabier F, Bouchard A., Brun E., Doerenbecher A.,Guedj S., Guidard V., Karbou F., Peuch V.-H., Puech D., Genthon C., Picard G., Town M., Hertzog A., Vial F.,Cocquerez P., Cohn S., Hock T., Parsons D., Powers J., Romberg K., VanAndel J., Deshler T., Haase J., Avallone L., Mechoso C.R., Tangborn A., Pellegrini A., Frénot Y. , Thépaut J.-P., Steinle P., 'The Concordiasi project in Antartica for the International Polar Year (IPY)'; The Bulletin of American Meteorological Society, january, 2010

Acknowledgements
Concordiasi was built by an international scientific group and is currently supported by the following agencies: Météo-France, CNES, IPEV, PNRA, CNRS/INSU, NSF, UCAR, University of Wyoming, Purdue University, University of Colorado and ECMWF. The two operational polar agencies PNRA and IPEV are thanked for their support at Concordia station and at the coast of Adélie Land. The NSF is thanked for its support at the McMurdo base. Concordiasi is part of the THORPEX-IPY cluster within the International Polar Year effort. Detailed information on Concordiasi is available on the web site "http://www.cnrm.meteo.fr/concordiasi/"

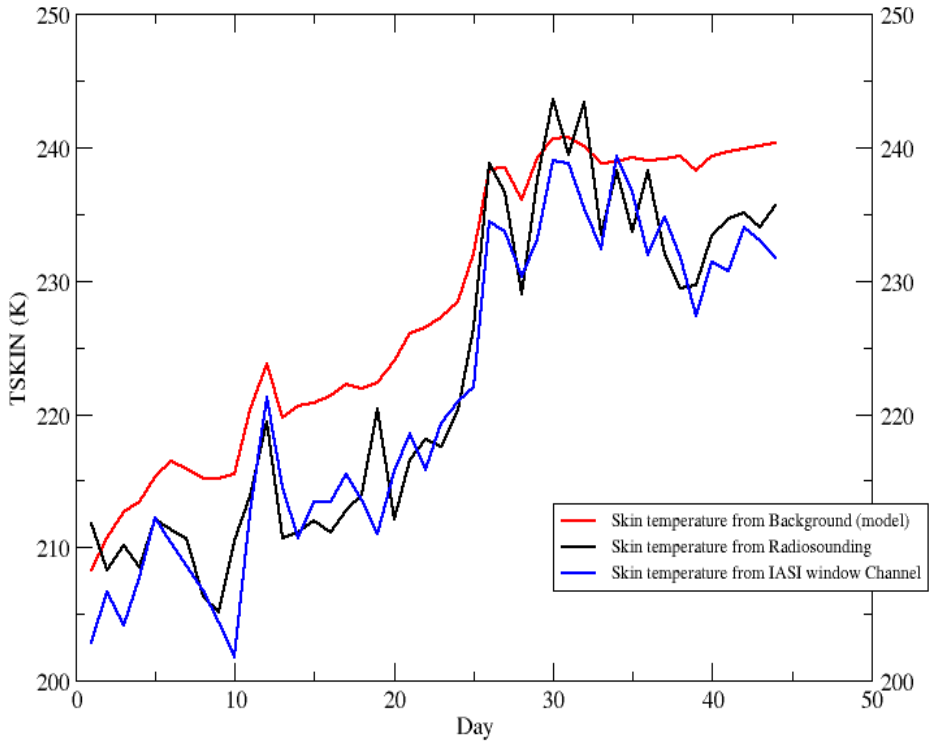

Figure 1: Skin temperature (K) from data in austral spring 2008 (44 cases between the 1st October to 29 November 2008 at 0hUTC) from Model (red line), radiosounding (black line), IASI window channel (blue line).

Assimilation of Aircraft Temperature Data in the JMA Global 4D-Var Data Assimilation System

Hiroshi Sako
Office of Observing Systems Operations, Japan Meteorological Agency
E-mail: h-sakou@met.kishou.go.jp

JMA had not assimilated commercial aircraft temperature data in the operational global data assimilation system because of temperature biases at cruising altitudes (particularly above 300 hPa). We developed a bias correction method to deal with this problem and studied the impact of aircraft temperature data assimilation in the JMA global analysis and forecast system using the new correction method.

The results showed a positive impact in global analysis and forecasting. Since the method's effectiveness was confirmed in the JMA high-resolution global data assimilation system (TL959L60), use of aircraft temperature data was implemented operationally in November 2009.

Quality control and bias correction for aircraft temperature data

Some NWP centers have pointed out that some aircraft data have temperature biases, most of which are warm ones.

In order to reduce such biases, a bias correction scheme was introduced to quality control for aircraft data (AMDAR and ACARS temperature reports, but not AIREP). This approach is known as a static bias correction scheme; when observed temperatures show noticeable biases in one-month statistics, the aircraft data for the next month are modified to reduce the calculated bias. The statistics are based on the difference between the reported temperature and the background temperature (O-B). JMA also employs a similar bias correction method for radiosonde data.

Additionally, when temperature data from an aircraft show biases larger than 2.5 K in one-month statistics, data from the aircraft are not used the next month. The aircraft reporting data with large temperature biases are blacklisted for exclusion from use due to doubtful data quality.

Experiments

Experiments were performed using the JMA low-resolution global data assimilation system (TL319L60). The two separate periods of 1 – 30 September 2008 and 1 – 31 January 2009 were studied. Nine-day forecasts were run from each 12 UTC analysis, making a total of 30 and 31 forecasts for each period, respectively. In both the control run and the test run, the JMA operational data set was used, including conventional data and satellite data. Aircraft temperature data were used only in the test run.

Results

Figure 1 shows the 500-hPa geopotential height anomaly correlation score for January 2009.

A positive impact was found in both the Northern Hemisphere (from day 1 to day 9) and the Southern Hemisphere (from day 1 to day 7).

Figure 2 shows the rate of improvement in the RMSE of forecast errors for 850-hPa temperature (T850), 500-hPa geopotential height (Z500) and 250-hPa wind velocity (Wspd250). Although the short-range forecast performance of T850 was somewhat worse, the forecast performance of Z500 and Wspd250 improved.

The impact was near neutral in September 2008 experiment, although the medium-range forecast (up to day 5) performance improved slightly (not shown).

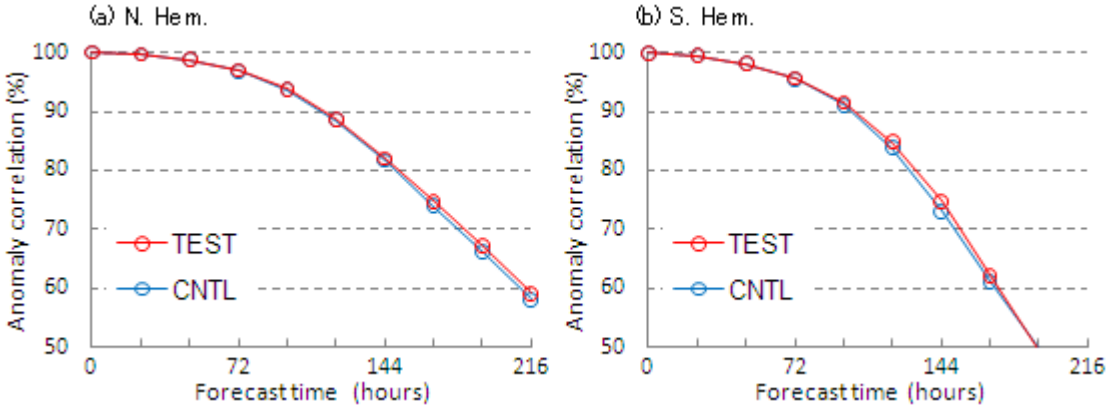

Figure 1. Anomaly correlations of 500-hPa geopotential height for the period 1 – 31 January 2009 (a) in the Northern Hemisphere (20°N – 90°N) and (b) in the Southern Hemisphere (20°S – 90°S). The test run is shown in red and the control run in blue.

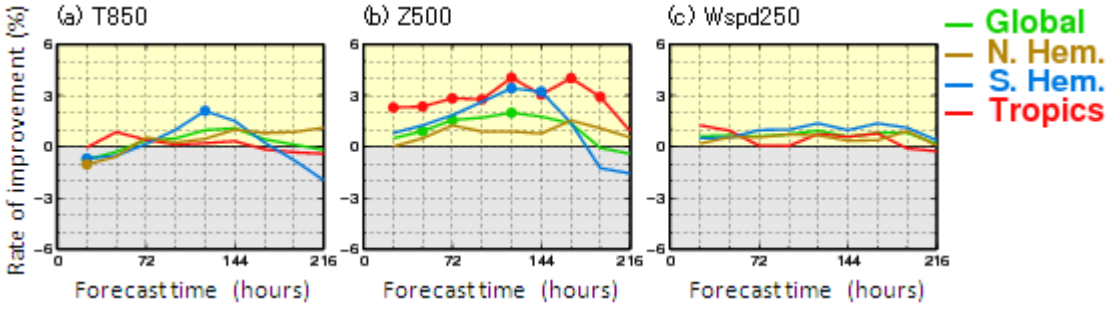

Figure 2. Rate of improvement in the RMSE of forecast errors for the period 1 – 31 January 2009 for (a) 850-hPa temperature, (b) 500-hPa geopotential height and (c) 250-hPa wind velocity. The improvement rate is defined as follows:

Improvement rate = (RMSEcntl - RMSEtest) / RMSEcntl

The dots on the lines indicate statistical significance.

References

C. Cardinali, L. Isaksen and E. Andersson, "Use and Impact of Automated Aircraft Data in a Global 4DVAR Data Assimilation System," *Monthly Weather Review*, Volume 131, Issue 8 (August 2003), pp. 1,865 – 1,877

Ensemble experiments of local heavy rainfall that occurred in Osaka, Japan, 5 September 2008

HIROMU SEKO[1], MASARU KUNII[2], TAKUYA KAWABATA[1]
and TAKEMASA MIYOSHI[2]

[1]*Meteorological Research Institute of Japan Meteorological Agency*
[2]*University of Maryland*

2

1. Introduction

Because local heavy rainfalls that occur in the urban area affect urban functions, accurate forecasts of generation and development of the convections are desired. Because of their small spatial scale and short duration, forecasts of local heavy rainfalls are more difficult than those of mesoscale heavy rainfalls. To reproduce local heavy rainfalls, techniques for producing accurate initial conditions, such as assimilation of radial wind of Doppler radar, have been developed. However, in most of these experiments, the horizontal convergences that were determined by boundary conditions were roughly reproduced, and then they were shifted to the observed positions by the assimilation of the observation data. Even if convergences surrounding local heavy rainfalls are not reproduced by deterministic forecasts, some members of ensemble forecasts can produce the convergence. In this study, the usefulness of ensemble forecast for reproduction of the mesoscale convergence is shown.

2. Osaka intense rainfall

Figure 1 shows rainfall distribution on 5 September 2008. Rainfall of which 1-hour rainfall amount exceeded 93 mm was observed in the southern part of Osaka (Fig. 1). When ensemble forecast with 20 members was performed with the NHM-LETKF (Miyoshi and Aranami, 2006), the spread was so large that the convergence positions were scattered, because of the insufficient observation data. However, one member, #005 roughly reproduced the position of convergence. Next, all members' outputs of this ensemble forecast were used as the first guess, and then radial wind of Doppler radars was assimilated. The heavy rainfall was reproduced when output of #005 was used as the first guess (Fig. 2). However, the heavy rainfall was not reproduced when other members' outputs were used. This result indicates that accurate boundary condition that determines the convergence position is needed to reproduce local heavy rainfall, and that NHM-LETKF is useful to reproduce the mesoscale convergence where local heavy rainfall is generated.

Besides the convective scale horizontal wind provided by Doppler radar, the convective scale water vapor and the loading of precipitation were introduced in the initial condition by following Seko et al. (2007). When initial condition was modified, the reproduced local heavy rainfall became closer to the observed one (not shown).

3. Summary

Ensemble forecast is useful to reproduce the mesoscale convergence where local heavy rainfall is generated.

References

Miyoshi, T. and K. Aranami 2006: Applying a Four-dimensional Local Ensemble Transform Kalman Filter (4D-LETKF) to the JMA Nonhydrostatic Model (NHM). *SOLA*, **2**, 128-131.

H. Seko, Y. Shoji and F. Fujibe, Evolution and Air flow Structure of a Kanto Thunderstorm on 21 July 1999 (the Nerima Heavy Rainfall Event). 2007, *JMSJ*, **85**, 455-477. .

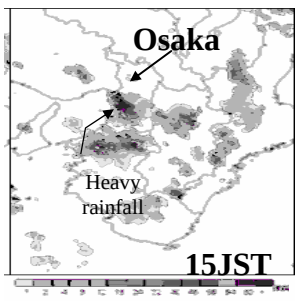

Fig. 1 Rainfall distribution observed by the conventional radars of JMA.

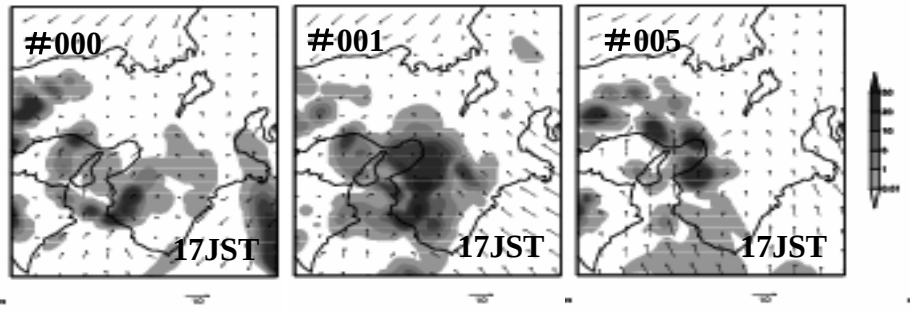

Fig. 2. Rainfall and horizontal wind distributions predicted from the assimilated fields of radial wind of Doppler radar. First guess of assimilation were the ensemble forecasts obtained by LETKF.

Data Assimilation of Side-looking Radio Occultation by Observing System Simulation Experiment

Seko[1], H., T. Tsuda[2], N. Yoshida[2] and Y.-H. Kuo[3]
Email: hseko@mri-jma.go.jp
[1]Meteorological Research Institute, Japan Meteorological Agency
[2]Research Institute for Sustainable Humanosphere, Kyoto University
[3]University Corporation for Atmospheric Research

Low earth orbit satellite (LEO) observes the signal of GPS satellite that came from the moving direction of LEO satellite, because the short shift of tangent point is required for precise estimation of tangent point profiles. If slant path data is used in the assimilation, occultation data of which the angle from the moving direction of LEO satellite (AFL) is large can be used in assimilation (Fig. 1). In general, impact of RO data is weak because the slant path data stretches for several hundred kilometers. For this reason, the total number of assimilated data should be increased by using 'side-looking' data. In this study, impact of side-looking data is investigated by OSSE.

We adopted the intense rainfall case that occurred at Kobe City as the target of OSSE (Fig. 2). Intense rainfall raised water level of Toga River, and then five people were drowned in the riverside park. In OSSE, truth data is needed to produce 'simulated slant data'. Analyzed fields of the intense rainfall case of Kobe City, which were obtained by the assimilation of ground GPS data and conventional data (Shoji et al 2009), were used as truth (Fig.3). We checked AFL distribution of occultation data (Fig. 4). Signals of data of which AFL was less than 60 degrees were received. However, profiles were not provided from the half of data of which AFL were larger than 50 degrees. Occultation data, of which AFL was larger than 60 degrees, is about 11% when satellite position data of the same day is used. Thus, total data that is expected to be received by side-flank observation becomes about 18%. There were several occultation data of which AFL were larger than 60 degrees near Alaska (Fig. 5). We used position of these occultation points that were shifted to Japan area. When the first guess and truth data was compared, path-averaged refractivity of truth below the height of 3 km is larger than that of first guess (Fig. 6). The reinforcement of rainfall is expected when this data is assimilated.

Figure 7 is the assimilation results of the simulated side-looking observation data. The intense rainfall was reproduced when the forecast was performed from the analysis field that was obtained by the assimilation of conventional data and 'simulated slant data'. Intensity and area of the rainfall became comparable to the observed one though the position was shifted westward.

Result of this study is summarized as follows: (1) when the side-looking data, of which AFL are large, are included in assimilation data, the analyzed fields is further improved, (2) however, the problems of hardware etc. are not considered. So, more experiment is needed under the more actual condition.

References

Shoji, Y., M. Kunii and K. Saito; 2009: Assimilation of Nationwide and Global GPS PWV Data for a Heavy Rain Event on 28 July 2008 in Hokuriku and Kinki, Japan, *SOLA*, **5**, 45-48.

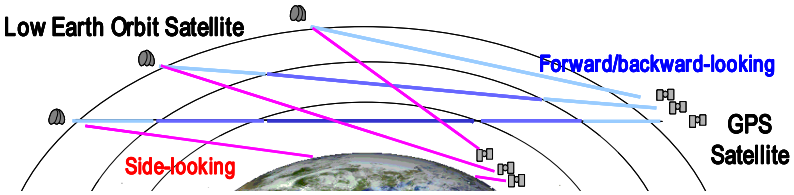

Fig1. Concept of side-looking observation

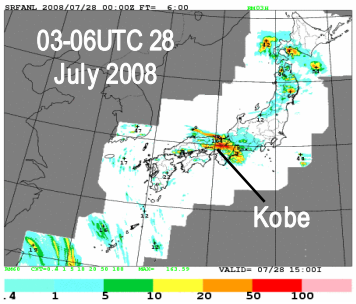

Fig.2 Target event of the observing system simulation experiment.

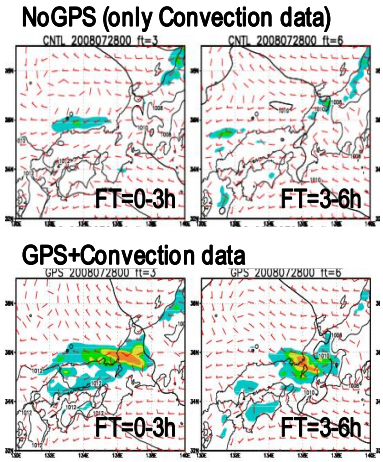

Fig. 3 Assimilation results of ground-based GPS data (After Shoji et al. 2009).

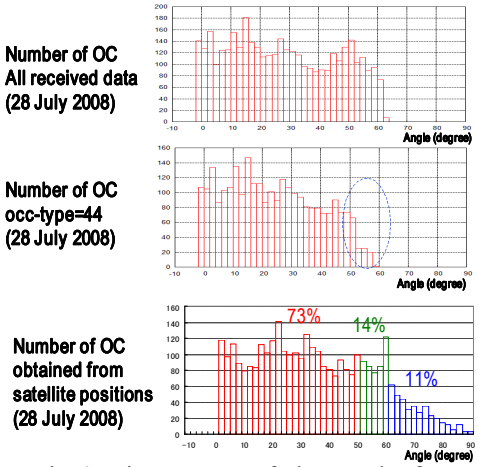

Fig.4 Histograms of the angle from moving direction of COSMIC of 28th July 2008.

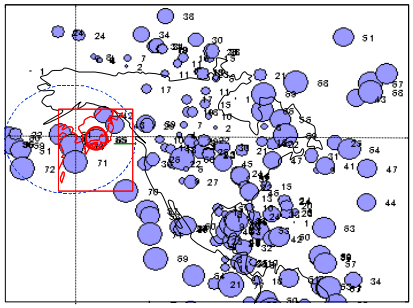

Fig. 5 Distribution of lowest tangent points during 12-15 UTC 13th September 2006.

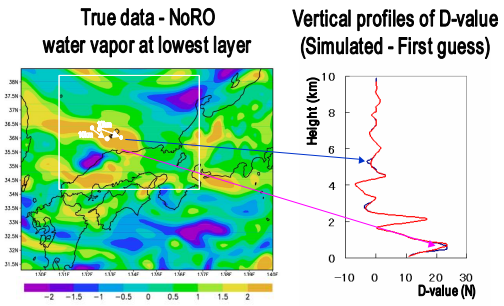

Fig. 6 (left) Difference between the true data and the assimilated fields of conventional data. (right) Vertical profile of difference of the true data and first guess data

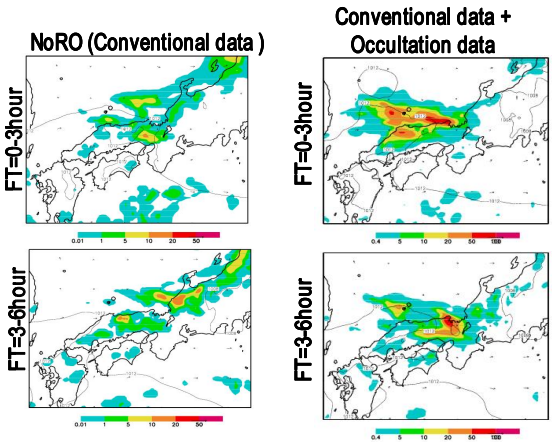

Fig. 7 Assimilation results of simulated side-looking observation data.

Operational use of Metop-A/ASCAT Winds in the JMA Global Data Assimilation System

Masaya Takahashi
Numerical Prediction Division, Japan Meteorological Agency
1-3-4 Otemachi, Chiyodaku, Tokyo 100-8122, Japan
E-mail: m_takahashi@met.kishou.go.jp

At the Japan Meteorological Agency (JMA), ocean surface vector winds derived from the Advanced SCATerometer (ASCAT) on board the Metop-A satellite have been assimilated in the operational global data assimilation (DA) system since 28 July 2009. ASCAT is an active C-band (5.3 GHz) scatterometer which has less sensitivity to rain than Ku-band (13.5 GHz) type (e.g., SeaWinds on board the QuikSCAT satellite, hereafter referred to as "QuikSCAT"). The six fan-beam antennas set on both sides of the spacecraft scan 550-km swaths separated by a gap of about 700-km. Wind data produced by the Royal Netherlands Meteorological Institute (KNMI) with a resolution of 50-km and 25-km cell spacing are used in this study. The increased data coverage using ASCAT wind vectors is expected to provide more valuable information to correct the initial field in one analysis.

Figure 1 shows two-dimensional histograms of JMA's first guess of ocean surface winds versus scatterometer winds derived from ASCAT and QuikSCAT. Both scatterometer winds closely match the Numerical Weather Prediction (NWP) winds, although high-speed ASCAT winds are underestimated.

In the preprocessing step of the DA, data thinning to approximately 100-km intervals and quality control are applied for the scatterometer winds. The former is to avoid using observations with errors that are highly correlated to each other. The latter is performed as follows: First, low-quality data are rejected by land/sea flag and KNMI quality control flag. Next, the most likely wind vector is selected in the ambiguity removal step using a median filter method initialized by nudging with JMA's first guess. Finally, data showing large departures of wind speed and direction from the first guess winds are screened.

To evaluate the impacts of ASCAT data on analysis and forecasting, observing system experiments in a low-resolution (TL319L60) global DA and forecast system were carried out. Figure 2 shows the improvement rate of the root mean square error against the initials for sea level pressure forecast in August 2008. All experiments with scatterometer data significantly improved forecast scores in the short-range forecast period over the Northern and Southern Hemispheres. The scores of the experiment assimilating both QuikSCAT and ASCAT were comparable with that using only one scatterometer, indicating that the use of at least one scatterometer (ASCAT) avoids the degradation of forecast scores even if QuikSCAT data become unavailable.

As ASCAT winds of which speed is lower than 15 m/s have good quality, they have been assimilated in operation since July 2009. However, the end of QuikSCAT nominal mission in November 2009 points to a need for assimilating ASCAT high wind speed data. A new usage of ASCAT employing a bias correction method for wind speed is currently under investigation.

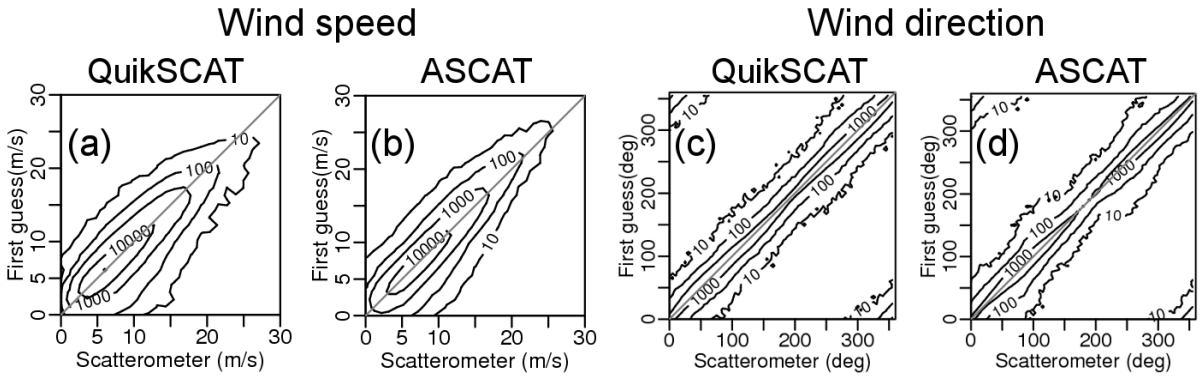

Figure 1: Two-dimensional histograms of JMA's first guess for sea surface winds versus scatterometer winds derived from ASCAT (b, d) and QuikSCAT (a, c) for 1 — 31 January 2009. Scatterometer winds after quality control and data thinning are used. The contour lines are on a logarithmic base-10 scale.

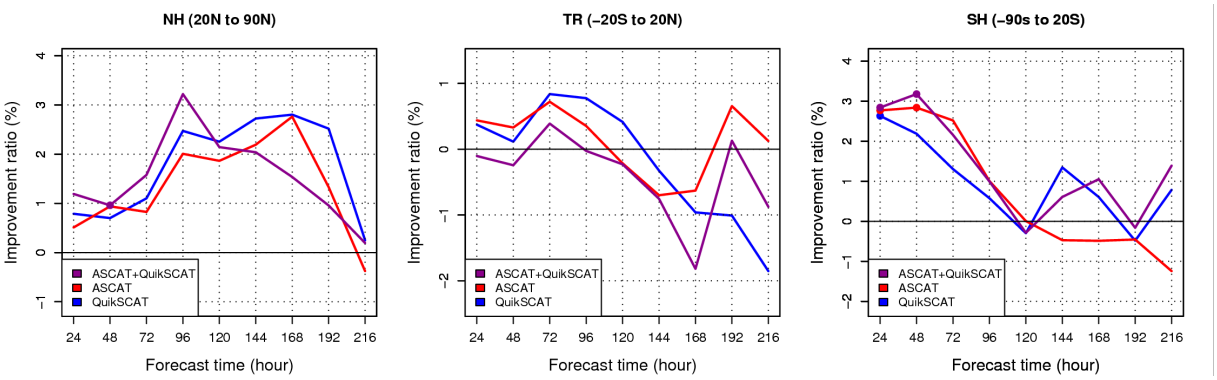

Figure 2: Improvement rate of the root mean square error (RMSE) against the initials for sea level pressure forecast, averaged over the Northern Hemisphere (left), the tropics (center) and, the Southern Hemisphere (right) for August 2008. The improvement rate is defined as (CNTL−TEST) / CNTL, where CNTL and TEST are the RMSEs of the experiments without and with scatterometer usage, respectively. The dots on the lines indicate statistical significance.

An Economical Approach to Four-dimensional Variational Data Assimilation

Bin Wang [1*], Juanjuan Liu[1], Bing Lu[1]

1. LASG, Institute of Atmospheric Physics, Beijing, China

*. Email: wab@lasg.iap.ac.cn

Ensemble-based 4DVar (En4DVar) includes the advantages of both standard 4DVar and EnKF. Currently, there have been efforts in the development of En4DVar family (e.g., Hunt et al., 2004; Qiu and Chou 2006; Liu et al. 2008; Tian et al. 2008; Zhang et al. 2009; Wang et al. 2010). One of the representative approaches in this family is the Dimension-Reduced projection 4DVar (DRP-4DVar) proposed by Wang et al (2010). B matrix used in DRP-4DVar is not only implicitly evolved within the time window but also explicitly developed from window to window. The implicit flow-dependent feature is derived from the equivalence between standard 4DVar and this approach in theory, while the explicit flow-dependence is decided by the estimation of B matrix using a number of initial-condition-reliant historical forecast samples.

The implementation of DRP-4DVar mainly includes three steps. The first step is to establish projection matrices using historical forecasts. In operational application, the historical forecasts are generally composed of two parts. One is the 72-hour forecasts initiated at the time 24 and 48 hours prior to the analysis time, and the other is an analog forecast selected from the past years. They are used to generate initial perturbations (IPs) by simply subtracting the background from them, and to produce simulated observations (SOs) and simulated observation increments (SOIs) using the observation operator and the basic state of SO. A quality control is included to select those weighted (or normalized) SOIs (WSOIs) derived from the 72-hour forecasts, which are significantly correlated with the weighted observation increment (WOI). The analog forecast is used to produce a higher-quality IP sample, whose corresponding WSOI is more significantly correlated with the WOI. The second step is to minimize the cost function in the sample space (or the coefficient space). After IP and its corresponding WSOI are projected onto the sample space using the projection matrices established at the first step, the original minimization of standard 4DVar in the control variable space whose dimension is about 10^6-10^8 can be easily completed in a 10^1-10^2-dimension sample space in this approach. The optimal solution to the minimization can be explicitly obtained, and does not require iterative procedure with adjoint technique. At this step, the construction of B matrix is very important. We use the IP samples generated at the first step to estimate B matrix to ensure its global flow-dependent feature. After it is projected from the control variable space onto the sample space, it becomes a low-dimensional and constant matrix. The third step is localization. Because the ensemble is composed of far fewer members, many spurious correlations between observation locations and model grids may appear. Thus, a localization technique as the one in EnKF is included to ameliorate the spurious long-range correlations. The details of DRP-4DVar can be found in Wang et al. (2010).

In the past two years, DRP-4DVar has been evaluated with assimilation experiments. Fig. 1 shows the results of assimilation-forecast experiments of typhoon. They are conducted with the Advanced Regional Eta Model (AREM), a limited area, hydrostatic primitive equation model, with 32 eta layers for all grid meshed with horizontal resolution of 37 km. Fengshen (2008 06TC) is chosen to complete two group experiments. One is control experiment (CTL) initialized at the analysis time (0000 UTC 24 June 2008) with 1°×1° National Centers for Environmental Prediction (NCEP) Final (FNL) Global Tropospheric Analyses. The other is DRP-BDA (DRP-4DVar-based bogus data assimilation) experiment that assimilates bogus surface pressures calculated according to Fujita formula into the first guess through DRP-4DVar. The assimilation window is 20 minutes, in which the same bogus surface pressures are used as observations every 2 minutes. Figure 1 gives the forecast of the 36-h track and intensity from CTRL and DRP as well as observations from 0000 UTC 24 to 0012 UTC 25 June 2008. CTL presents a track error of 39 km at the start of the window and of 452 km after

36-hour forecast (Fig. 1b). In contrast, DRP-BDA greatly improved the prediction of movement. The track error is only 10 km at initial time and 32 km after 36 hours (Fig. 1b). Furthermore, it produces a much better forecast landing time and a central sea level pressure closer to the observed than CTL (Fig. 1c).

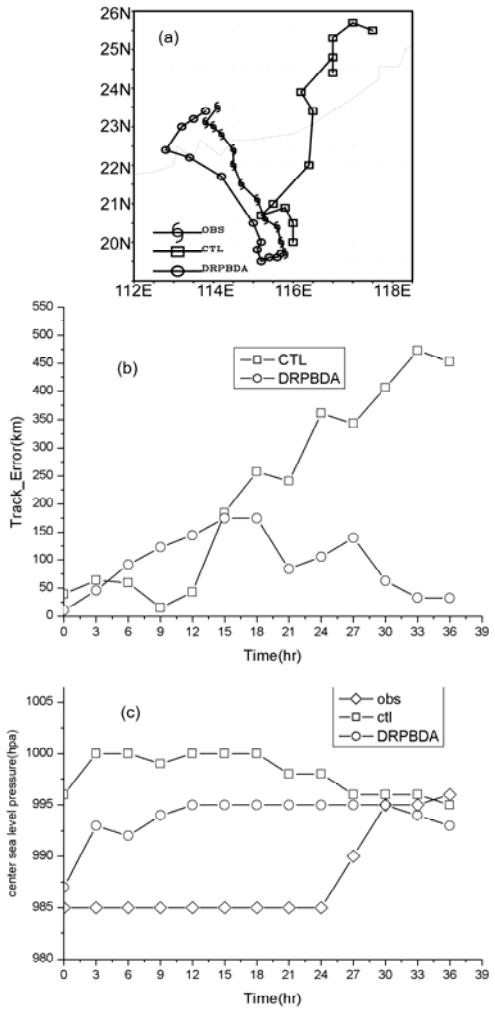

Fig. 1 Forecasts of Typhoon Fengshen for the entire 36-hour forecast period from 0000 UTC 24 June to 0012 UTC 25 June 2008 at 3-hr intervals: (a) track (km), (b) track error (km), and (c) central sea level pressure (hPa).

Reference

Hunt, B. R., and co-authors, 2004: Four-dimensional ensemble Kalman filtering. *Tellus*, **56**A , 273–277.

Liu, C. S., Q. Xiao, and B. Wang, 2008: An Ensemble-based four-dimensional variational data assimilation scheme: Part I: Technical formulation and preliminary test. *Mon. Wea. Rev*., **136**, 3363-3373.

Qiu, C.-J., and J.-F. Chou, 2006: Four-dimensional data assimilation method based on SVD: Theoretical aspect. *Theoretical and Applied Climatology*, ***83,*** 51-57.

Tian, X.-J., Z.-H. Xie, and A.-G. Dai, 2008: An ensemble-based explicit four-dimensional variational assimilation method. *J. Geo. Res.*, **113**, doi:10.1029/2008JD010358 (in press).

Wang, B., J. Liu, S. Wang, W. Cheng, J. Liu, C. Liu, Q. Xiao, and Y.-H. Kuo, 2010: An economical approach to four-dimensional variational data assimilation. *Adv. Atmos. Sci.*, doi: 10.1007/s00376-009-9122-3.

Zhang, F., M. Zhang and J. A. Hansen, 2009. Coupling ensemble Kalman filter with four- dimensional variational data assimilation, *Adv. Atmos. Sci*. **26**, 1-8.

Assimilation of radar reflectivity in the AROME model

By Eric Wattrelot

CNRM/GAME, Météo-France and CNRS
42 av Coriolis
31057 Toulouse
France
eric.wattrelot@meteo.fr

These last years, Météo-France has developed a Numerical Weather Prediction (NWP) system at convective scale that is running operationally since the 18th December 2008. This system, called AROME, covers metropolitan France with a 2.5 km horizontal resolution. High frequency observations to initialize at similar time and space scales are needed because small scales do not just adapt to large scales. Indeed, high resolution models represent key convective cells with a significant small-scale memory: older convection (as gust fronts or cold pools) may influence the development of new convective systems. Radar reflectivity is capital to provide such high-resolution information about precipitating patterns. Studies of precipitating systems with the assimilation in the AROME model of volumic radar reflectivities from the national ARAMIS network showed a better description of qualitative and quantitative precipitation short term forecasts, especially for cases of good vertical sampling of the atmosphere.
Relative humidity profiles from radar reflectivities are firstly retrieved and then assimilated in the 3DVar AROME as pseudo-observations. This method has the main advantage to use vertical information from useful volumic radars. As both rainy and non-rainy observation are used, either precipitations are produced or the model dries up. In figure a, one can see the impact on a relative humidity analysis of the assimilation of reflectivities from high altitudes (rain does not reach the ground). The propagation of the information is consistent with the observed spatial scales.

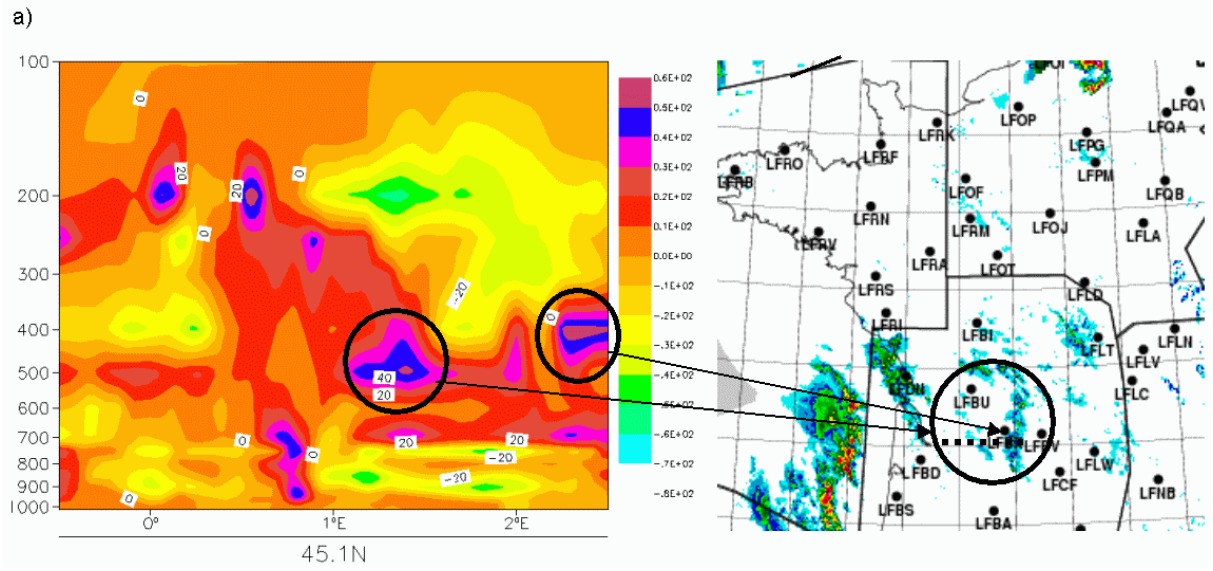

Figure a caption: Left, vertical cross-section (corresponding to the dashed line on the radar composite map right) from a relative humidity difference between an experience with assimilation of radar reflectivities and an experience without reflectivity being assimilated.

Daily evaluations of this assimilation have shown positive results in a pre-operational context. In particular a positive impact is found for very short range precipitation forecast scores. Results from such an experiment, running from the 15th of April 0000 UTC to the 23rd of April 2009 0000 UTC, are shown hereafter. During this period, important precipitation associated with a surface cold front crossed France eastwards on the 16th of April. At that time, an unstable air mass over France was associated with a large low on the Near Atlantic which was getting close to France. Associated with the cold upper-air and front over France, embedded and post-frontal convective precipitation occurred during several days. Fig. b shows positive scores for 6-hour accumulated precipitation forecasts against rain gauges, between 3-h and 9-h forecasts when the reflectivities are assimilated (REFL against CTRL). An improvement of forecast scores for other parameters (such as wind) over long periods is also observed (not shown here).

b)

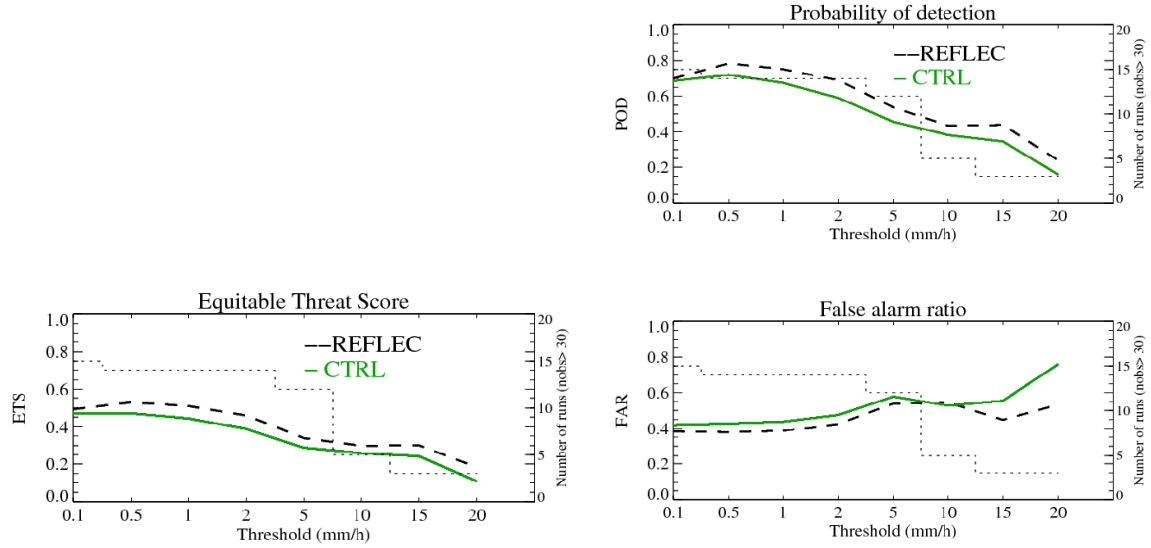

Figure b caption: Left: averages of Equitable Threat Scores (ETS) for 6-hour precipitation forecasts against raingauges, between 3-h and 9h forecasts (at 00h and 12h UTC from 15 April to 23 April 2009 00h), as a function of threshold (mm/h) for CTRL (green line) and REFL (black dashed line). The thin dashed line represents the number of forecasts taken into account in the calculations, i.e., for which the number of observations above the threshold exceeds 30. Top right: idem for Probability of detection (POD) and Bottom right: idem for False Alarm Ratio (FAR).

Since the end of 2008, the assimilation of reflectivities has been systematically evaluated, by means of a radar product optimized for the Arome model (Doppler winds and reflectivities). Data from the 24 radars network are now assimilated in the pre-e-suite but at this moment neither the very low reflectivities from the lower troposphere (echoes which may be still unidentified anomalous beam propagation) nor the lowest elevations affected by high values of topographical beam blockage are assimilated.

Wattrelot E, Caumont O., Pradier-Vabre S., Jurasek M. and Günther Haase , 1D+3DVar assimilation of radar reflectivities in the pre-operational AROME model at Météo-France. ERAD2008. *Proceedings of the fifth European conference on radar in meteorology and hydrology.*

Caumont, O. V. Ducrocq, E. Wattrelot, G. Jaubert, S. Pradier-Vabre, 1D+3DVar assimilation of radar reflectivity data: A proof of concept, *Tellus, DOI : 10.1111/j.1600-0870.2009.00430.x. In press.*

Improvement of Conventional Observation Data Usage in the JMA Mesoscale 4D-VAR Data Assimilation System

Koichi Yoshimoto
Numerical Prediction Division, Japan Meteorological Agency
1-3-4 Otemachi, Chiyoda-ku, Tokyo 100-8122, Japan
(E-mail: k-yoshimoto@met.kishou.go.jp)

1. Introduction

In JMA, the operational mesoscale data assimilation system based on a hydrostatic model (Meso 4D-Var) (Ishikawa and Koizumi, 2002) was replaced with a four-dimensional variational data assimilation system based on JMA's non-hydrostatic model (JNoVA) (Honda and Sawada, 2008) in April 2009. Consequently, there is a need to examine the usage of conventional observation data and the quality control (QC) method for JNoVA.

2. Observation Error and Observation Error Correlation

We estimated the level of observation error and observation error correlation suitable for JNoVA through a statistical study. In the study of Desroziers et al. (2005), observation error and observation error correlation were estimated from the covariance of observations minus the first guess (O-B) and observations minus the analyzed value (O-A). Figure 1 shows the estimated observation errors for temperature, U-component and V-component wind, and relative humidity. Figure 2 shows the observation error correlation for AMDAR (Aircraft Meteorological DAta Relay). In JNoVA, the estimated observation error is smaller than the current observation error estimated under the hydrostatic Meso 4D-Var system. Accordingly, the conventional observation error was investigated along with an experiment for estimated radiosonde observation error. In addition, the thinning distance of AMDAR was estimated along with an experiment in which a two-layer thinning distance was employed, and values of 60 km for reports above 500 hPa and 15 km for those below 500 hPa were obtained.

3. Variational Quality Control

As a new way of ensuring quality, we developed variational quality control (VarQC; Andersson and Järvinen, 1999). The VarQC approach uses the probability density function (PDF) of observation in which the Gaussian function is changed to a statistically proper function considering rough errors in observation. The new PDF of observation (p^{QC}) is given as follows:

$$p^{QC} = (1 - A)N + AF \quad (1)$$

$$N = \frac{1}{\sqrt{2\pi}\sigma_o} \exp\left[-\frac{(y_o - Hx)^2}{2\sigma_o^{\,2}} \right] \quad (2) \qquad F = \frac{1}{2d\sigma_o} \text{ , if } |y_o - Hx| < d\sigma_o \text{, otherwise 0} \quad (3)$$

where A is the prior probability of gross error, y_o is the observation, x is the model state, H is the observation operator, σ_o is the observation error's standard deviation, and d is the maximum number of standard deviations allowed for gross error.

Here, VarQC parameter A was estimated from a statistical study from April 7 to July 31, 2009, and d is defined as 5.0 according to Andersson and Järvinen (1999).

4. Improvement of forecast results

Experiments were performed over a one-week period with heavy rainfall during the Baiu season in 2009. Figure 3 shows the equitable threat score (ETS) of three-hourly accumulated precipitation forecasts for each precipitation threshold. This outcome demonstrates that the revised observation error and thinning distances of AMDAR and VarQC gave better results.

References

Andersson, E. and H. Järvinen, 1999: Variational Quality Control. *Quart. J. Roy. Meteor. Soc.,* **125**, 697 – 722

Desroziers, G., L. Berre, B. Chapnik and P. Poli, 2005: Diagnosis of observation, background and analysis-error statistics in observation space. *Quart. J. Roy. Meteor. Soc.,* **131**, 3,385 – 3,396

Honda, Y. and K. Sawada, 2008: A New 4D-Var for Mesoscale Analysis at the Japan Meteorological Agency. *CAS/JSC WGNE Res. Activ. Atmos. Oceanic Modell.*, **38**, 01.7 – 01.8

Ishikawa, Y. and K. Koizumi, 2002: One month cycle experiments of the JMA mesoscale 4-dimensional variational data assimilation (4D-Var) system. *CAS/JSC WGNE Res. Activ. Atmos. Oceanic Modell.*, **32**, 0126 – 0127

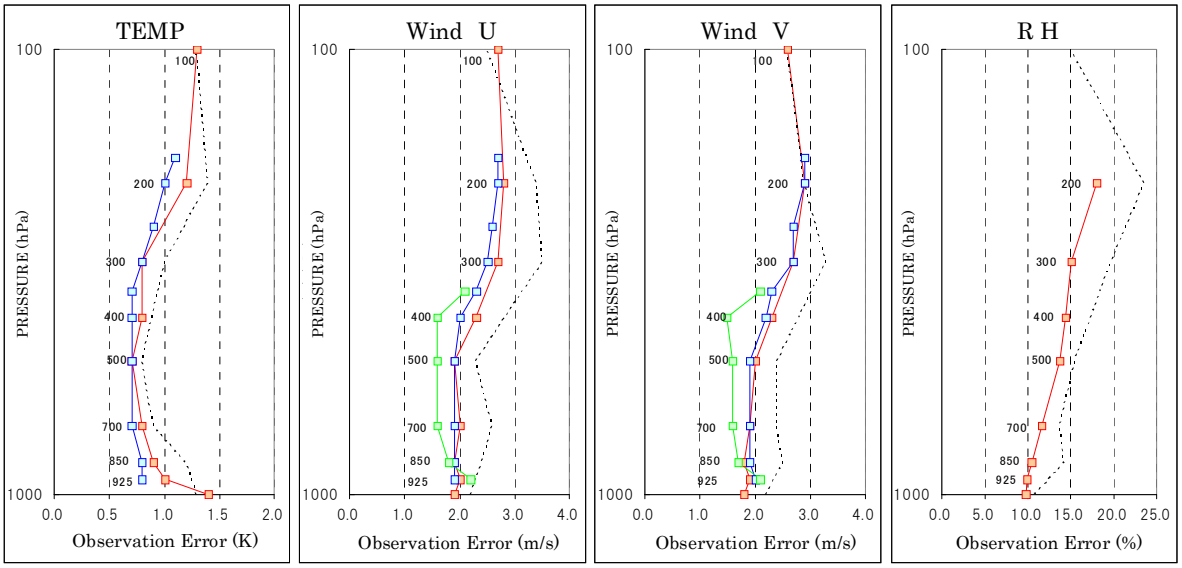

Figure 1: Estimated observation errors. The statistical period is from April 7 to July 26, 2009. The red lines are radiosonde values, the blue lines aircraft values, the green lines wind profiler values, and the dashed lines show the observation error currently used in JNoVA.

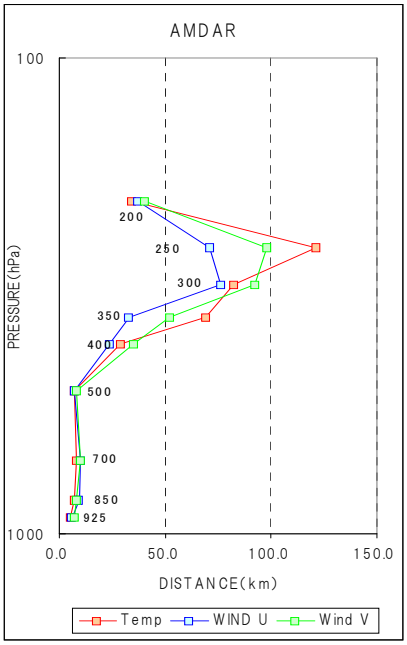

Figure 2: Estimated observation error correlation. The statistical period is from April 7 to July 26, 2009. The red line is for temperature, the blue line is for U-component wind, and the green line is for V-component wind.

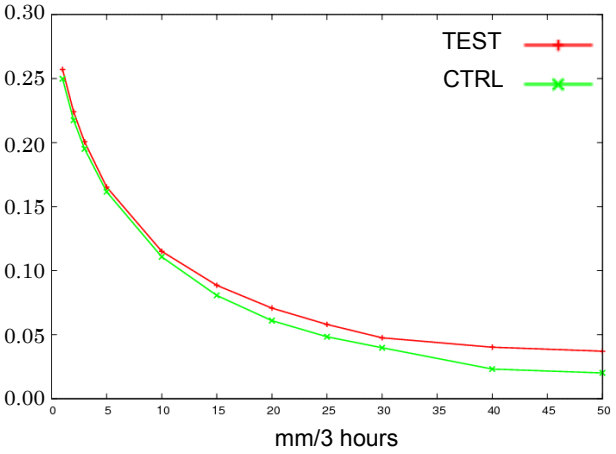

Figure 3: Equitable threat scores for three-hourly accumulated precipitation forecasts. The red and green lines show the results for TEST and CTRL, respectively. The horizontal axis is the threshold value of the rainfall amount.